Università degli Studi del Piemonte Orientale
"Amedeo Avogadro"

Dipartimento di Scienze del Farmaco

Dottorato di Ricerca in Scienza delle Sostanze Bioattive
XXVI ciclo a.a. 2010-2013

Celecoxib Targets CML Blasts Proliferation in a COX-2 independent manner

Beatrice Riva

Supervised by Prof. Pier Luigi Canonico and Prof. Fabrizio Condorelli

PhD program co-ordinator Prof. Luigi Panza

To my Parents…

To my Aunt…

and

To my little Niece…

"There is a driving force more powerful than steam, electricity and atomic energy: The Will"

Albert Einstein

Contents

Chapter 1:

Introduction

1. Introduction

1.1 Chronic Myeloid Leukaemia

Chronic myeloid leukaemia (CML) is a clonal myelo-proliferative disorder of the hematopoietic stem cell [1]. It is a neoplastic disease characterized by the increased and unregulated growth of white blood cells in spleen, liver, peripheral blood and, more rarely, in the lymph nodes. CML it is also characterized by an impairment of the granulocytic lineage in their capacity to differentiate. Consequently, the peripheral blood cell profile shows an increased number of granulocytes and their immature precursors, including occasional blast cells [2,3].

Incidence of CML is rare, about 1 o 2 cases per 100.000 people every year, with a prevalence in older people as median age at diagnosis is about 50 years.

Men are affected more frequently than women, although female patients seem to have a survival advantage. No obvious geographical or ethnic differences exist, but differences in management strategies between countries could be dependent on the availability of expensive drugs and modern diagnostic technologies [4].

Diagnosis of CML is generally straightforward. In most cases the diagnosis is made on the basis of the characteristic blood count (white blood cells count > 25.000/μL) and upon exclusion of myelofibrosis or myelodysplasia.

CML typically evolves in three distinct clinical stages: chronic phase, accelerate phase, and blast crisis. The chronic, or stable, phase lasts several years and is characterized by an excessive number of myeloid precursors and mature cells in bone marrow, peripheral blood and extra-medullary sites [1,5]. The accelerate phase last 4 to 6 months and is characterized by an increase in disease burden and in the percentage of progenitor/precursor cell that are detected in the peripheral blood.

Historically, within an average of 4 to 6 years, the disease evolves from accelerate phase to an, invariably fatal, acute disease, also known as blast crisis. This crisis last only a few months and is characterized by the rapid expansion of a population of myeloid or lymphoid blasts [1,5,6].

From a patho-physiological point of view, the immediate cause of CML was discovered in 1960 by Nowell and Hugerford, who described the presence of a small acrocentric chromosome, named Philadelphia chromosome (Ph) after the hometown of its discovery, in blood cells isolated from patients with CML [6]. In 1973, Rowley showed that this abnormal Ph chromosome was a result of a reciprocal translocation between the long arms of chromosome 9 and 22 t(9;22)(q34;q11). In details, it was shown that a long arm of the *abelson* (*abl*) gene, located on chromosome 9, is translocated to the *breakpoint cluster region* (*bcr*) gene on chromosome 22 (Figure 1).

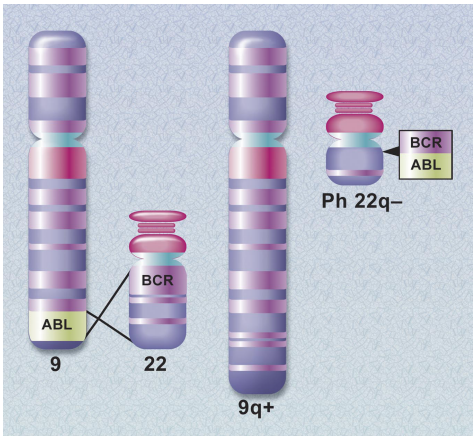

Figure 1. Schematic diagram of the translocation that creates the Philadelphia chromosome

The *abl* and *bcr* genes reside on the long arms respectively of chromosome 9 and 22. *bcr-abl* gene is formed on the derivative chromosome 22 (Philadelphia chromosome), as result of the (9:22) translocation.
Illustration by *Druker Brian J., Blood, 2008 December; 112 (13); 4808-4814.*

This translocation generates the *bcr-abl* fusion gene, which is translated, in the majority of the patients with CML, in a 210kDa protein indicated as $p210^{BCR-ABL}$ [1,6]. Expression of $p210^{BCR-ABL}$ has been shown to be necessary and sufficient for the malignant transformation of of CML blood cells [1, 2].
Alternatively, other two BCR-ABL proteins may be generated, depending on the region of the breakpoint on the *bcr* gene, although these are detected in classic CML only occasionally.
BCR-ABL, unlike the normal p145 c-Abl, is predominantly localized in the cytoplasm and has constitutive tyrosine kinase activity, essential for cell transformation. The cytoplasmic localization of the oncoprotein allows the assembly of phopshorylated substrates in multiprotein complexes that transduce mitogenic and antiapoptotic signals [1].
Ectopic expression of BCR-ABL in growth factor-dependent cell lines activates numerous signal transduction pathways responsible for acquisition of growth factor independence and reduced susceptibility to apoptosis. For instance, it is known from literature that the ectopic expression of BCR-ABL enables phosphatidylinositol-3 kinase (PI-3K)-dependent activation of Akt. This cascade of events plays a critical role in BCR-ABL-driven transformation since it regulates the subcellular localization or activity of several effectors with relevance in cell proliferation and viability, such as: BAD, MDM2, IkB-kinase-α and members of the Forkhead family of transcription factors.
It is also assumed that, BCR-ABL supports cell proliferations by reducing the nuclear localization of $p27^{KIP}$ and increasing the expression of Cdk2.
On the other hand, BCR-ABL may induce leukeamogenesis also stabilizing cyclin D1 and β-catenin, through the inactivation of GSK-3β [7].

Nonethelss, BCR-ABL-dependent activation of STAT5 probably represents the most critical event for the maintenance of CML, since the direct phosphorylation of this protein enables its transcriptional program toward transformation (Figure 2).

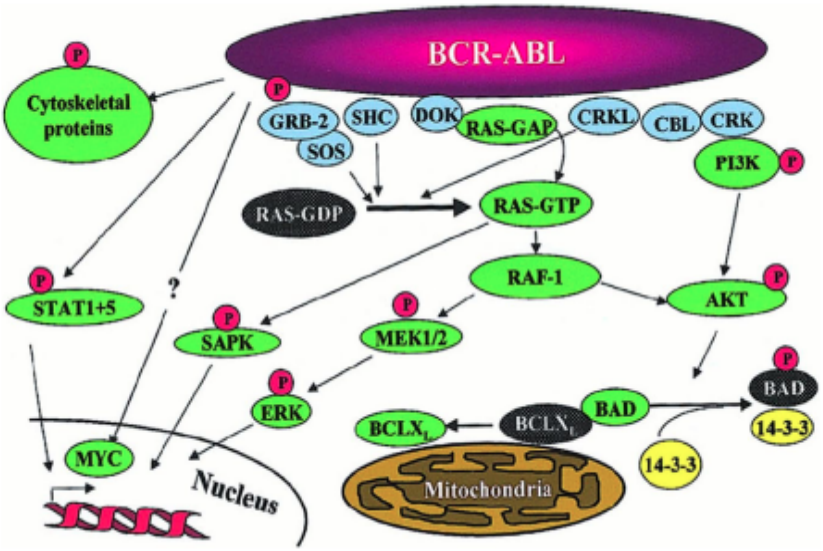

Figure 2. Signaling pathways impacted by BCR-ABL expression

Schematic representations of the main BCR-ABL activated pathways regulating survival and proliferation of BCR-ABL-transformed hematopoietic cells. Note that is a simplified diagram. Illustration by *Deininger Michael W. N., et al., Blood, 2000 November; 112 (13): 3343-3356.*

1.2 CML Therapy

Before the discovery of Tyrosine Kinase Inibhitor (TKI) class of drugs, the conventional treatments for CML were based on the use of cytotoxic chemotherapies, in particular busulfan and hydroxyurea. Later, in 1980, allogenic stem cell transplantation became the only curative treatment for CML, although this therapeutic option is accessible to a limited number of patients due to difficulties in enrolling suitable donors [(6)]. Also in the 80s, interferon alpha was introduced to treat patients ineligible for transplant, progressively replacing both busulfan and hydroxyurea in the management of CML for improved survival and durable cytogenetic responses, in approximately one-third of the patients [(8)]. In 1998, CML therapy was revolutionized by the introduction on the market of the first TKI, imatinib (Gleevec®; Figure 3).

Imatinib is a small molecule that targets the BCR-ABL tyrosine kinase by competitively inhibiting the binding of adenosine triphosphate (ATP) to the catalytic site of the ABL kinase. Subsequent studies, also showed that imatinib was able to inhibit other tyrosine kinases, in particular c-Kit and PDGFβ-R (Figure 4) [(7)].

As regarded the treatment CML patients bearing the Ph chromosome, imatinib showed its high efficacy as evaluated in Phase I and II clinical trials; this caused an accelerated FDA approval, in May 2001, for treating Ph+ CML patients during blast crisis and accelerate phase, or those in chronic phase, after failure of treatment with Interferon-alpha. The development of these target therapies overcame the limitations of the previous conventional treatments; indeed imatinib demonstrated a good tolerability and superiority in terms of hematologic and cytogenetic responses, as compared to Interferon-alpha [4, 9].
Although in most of the cases imatinib was able to control the chronic phase of CML, some patients relapsed, after a period of improvement, or progressed to accelerated phase or blast crisis.

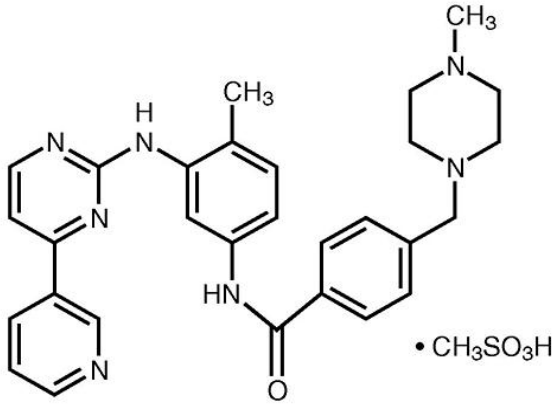

Figure 3. Chemical structure of imatinib

Illustration by *www.theodora.com web site*

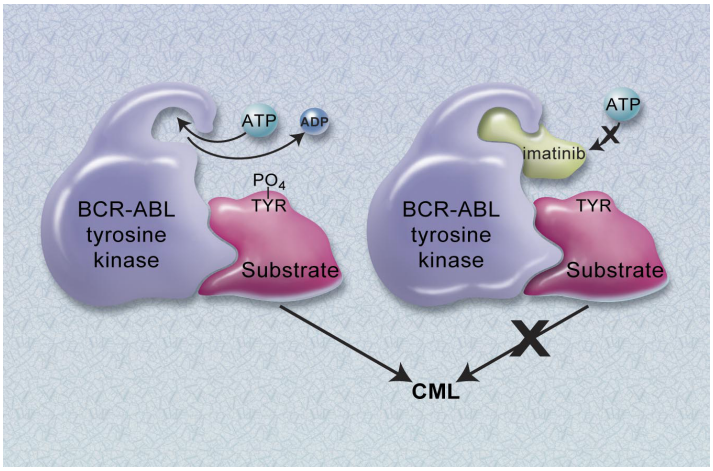

Figure 4. Mechanism of action of imatinib

The constitutively active BCR-ABL tyrosine kinase function by transferring phosphate from ATP to tyrosine residues, that causes excess proliferation of myeloid cells in CML (left panel).
Imatinib blocks the binding of ATP to BCR-ABL, thus inhibiting the kinase activity of the protein (right panel).
Illustration by *Druker Brian J., Blood, 2008 December; 112 (13): 4808-4814.*

Although the mechanisms responsible for resistance to imatinib are still not completely known, it has been demonstrated that treatments with this compound may lead to selection of cells overexpressing BCR-ABL or expressing normal levels of BCR-ABL but with mutations in the ABL kinase domain, e.g. T315I and Y253H mutations [10,11].
BCR-ABL-independent mechanisms are the second major category of resistance to imatinib. In particular, a decreased intake of imatinib or an eccessive efflux, as caused by the increased expression of P-glycoprotein (Pgp)[11], may be responsible for maintaining intracellular concentration of this drug just below the therapeutic level.

On the other hand, BCR-ABL-independent activation of signaling pathways such as Src/Ras/Raf/MEK/Lyn, STAT3/5, Wnt/β-catenin, FoxO and SIR1, which conceivably coexist in the same cell, may also play a role in CML resistance to therapies and progression of the disease [2,4,5].
In order to overcome resistance to imatinib and improve the prognosis of patients with CML, second-generation inhibitors of BCR-ABL have been introduced on the market, such as dasatinib and nilotinib.
Dasatinib is a piperazinyl derivate that potently targets also Src and Abl kinases as well as most of the mutated form BCR-ABL (with the exclusion of T315I).
Nilotinib is an aminopyridine derivate that inhibits the tyrosine kinase activity of the unmutated and most mutated form of BCR-ABL, more potently and more selectively than imatinib, although sparing the T315I mutated oncoprotein. Consequently, Dasatinib and Nilotinib are highly effective in treating many but not all the cases of imatinib-resistant CML [9]. As consequent to these aspects of TKI-resistance, allogeneic stem-cell transplantation is the only treatment that can lead to a complete cytogenetic remission, but often the main disadvantage of this therapy is associated to *"graft vs host"* reactions that, during treatment, can induce the death of approximately 30% of patients.

Recently, investigations on the mechanisms that cause the escape of CML from cures unveiled the existence of a primitive sub-set of cells endowed with stem capacity, thus named leukaemic stem cells (LSCs). LSCs are the transformed counterpart of normal hematopoietic stem cells (HSCs), since they are equipped with very peculiar capacities such as: self-renewal (in supportive microenvironment) and quiescence, characterized by a lengthy G1 phase of the cell cycle and highly efficient DNA-repair response, that provides resistance to either canonical cytotoxic chemotherapies and "target therapies", such TKI, directed towards fast proliferating cells. Indeed, the population of cells, which is involved in chronic phase initiation of CML, expresses surface markers that are in common with HSCs, i.e. $CD34^{+}CD38^{-}CD90^{+}Lin^{-}$, and partially preserve their ability to undergo a myeloid differentiation, thus leading to myeloid progenitor expansion. Upon shifting to the blast crisis stage of the disease, leukemia is fueled the expansion of the granulocyte-macrophage progenitor (GMP) population, which presents an amplified BCR-ABL expression. The malignant GMPs are reprogrammed to regenerate via aberrant activation of self-renewal and survival pathways, determining the therapeutic resistance [12].
This type of resistance may be a consequence of the genetic instability promoted, at least in part, by the activity of BCR-ABL on its own. Indeed, recent studies demonstrated that LSCs resistance to TKIs is not consequent to an altered binding of these drugs to BCR-ABL but to an aberrant activation of additional signaling pathways, both intrinsic to LSCs and controlling their survival and self-renewal, or extrinsic to them, although capable to support the hematopoietic microenvironments [13]. Indeed, cumulative research efforts brought to the demonstration that inactivation of apoptosis and induction of autophagy, through an interference on Wnt/β-catenin or glycogen synthase kinase-3β (GSK-3β) signal pathways, may be key cell-intrinsic factors that promote LSCs persistence and TKI

resistance. Adding to this, cell-extrinsic factors may sustain CML through production, by the hematopoietic microenvironments (bone marrow niche), of mediators that promote cell migration and protection of LSCs (Figure 5)[12].

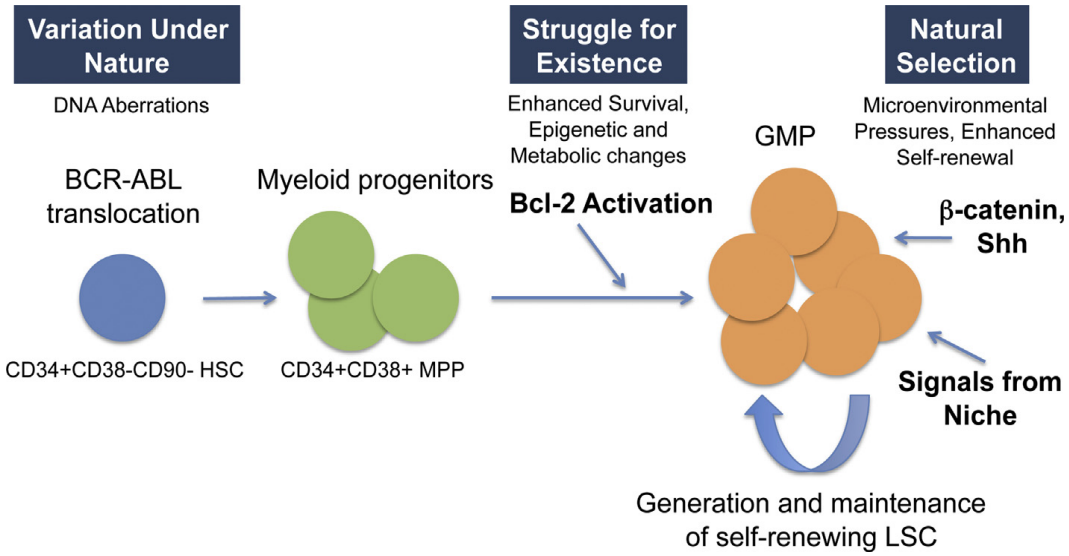

Figure 5. Model of LSCs evolution

The molecular evolution of hematopoietic stem cells (HSCs) into LSCs initiate with the BCR-ABL translocation occurring at the stem cell level, followed by the expansion of the myeloid progenitors. The acquisition of additional signal transduction abnormalities such as over-expression of Bcl-2 or β-catenin and dependence from Wnt signaling allows enhanced survival and self-renewal capacity of the granulocyte macrophage progenitor (GMP) population. These cell-intrinsic alterations induce LSCs expansion and survival, only in presence of supportive microenvironments.
Illustration by *Crews L.A., Jamieson C.H.M. Cancer Letters, 2013; 338 15-22.*

According to what described above, in the close future the next therapeutic goal is to eradicate the disease by implementing the use of TKIs (the actual golden standard in CML treatment), with drugs designed to target both cell-extrinsic and cell-intrinsic pathways sustaining LSCs life cycle [6, 9, 12].

1.3 LSCs self-renewal and the Wnt/β-catenin/Tcf/Lef signaling pathway

Many studies have been published that were focused on understanding the molecular mechanisms that allow CML stem cells to survive and that, once targeted, would enable their eradication or sensitization to TKIs and other antileukaemic drugs. Among these candidate pathways, those controlled by ALOX5, sonic hedgehog (SHH), STAT5, TGF-β and in particular Wnt were considered the most attractive [9, 12, 14].
The Wnt family of secreted protein is composed of at least 19 isoforms of activating ligands for two distinct signaling pathways.

The “non-canonical” Wnt signaling pathway is characterized by a β-catenin independent mechanism that influence cell polarity, division and migration during development [8,15].
On the other hand, the “canonical” Wnt signaling pathway controls the amount of the transcriptional co-activator β-catenin protein that drives specific gene expression programs. As such, several biological processes can be orchestrated, including cell fate determination, cell proliferation, stem cell maintenance, tumorigenesis and cancer progression [16]. The key regulatory step of this pathway involves the phosphorylation, ubiquitination and subsequent degradation of β-catenin [16,21].
Specifically, in the absence of Wnt (**WNT-off state**, Figure 6), β-catenin protein is constantly degraded in the cytoplasm by the action of Axin complex, composed of the scaffolding protein Axin, the tumor suppressor *adenomatous polyposis coli* (APC) gene product, the casein kinase 1 (CK1), and the glycogen synthase kinase 3 (GSK-3β). Axin coordinates sequential phosphorylation of β-catenin by CK1α, on serine 45, and by GSK-3β, on threonine 41, serine 37 and serine 33. Phosphorylation of β-catenin on serine 33 and 37 creates a binding site for β-Trcp (an E3-ubiquitin ligase), thus enabling ubiquitination and proteasomal degradation of β-catenin. Moreover, the *regulator of G protein* (RGS) domain within Axin allows interaction with β-catenin through APC [22,23,24].
The continuous degradation of β-catenin through this cascade of events prevents its translocation in the nucleus and, consequently, interaction with members of the *T cell factor/lymphoid enhancer factor* (Tcf/Lef) family of proteins. Accordingly, Wnt-driven gene transcription is repressed by the binding of the transcriptional corepressor Groucho/TEL to Tcf/Lef proteins, and the recruitment of histone deacetylases (HDAC) [23].

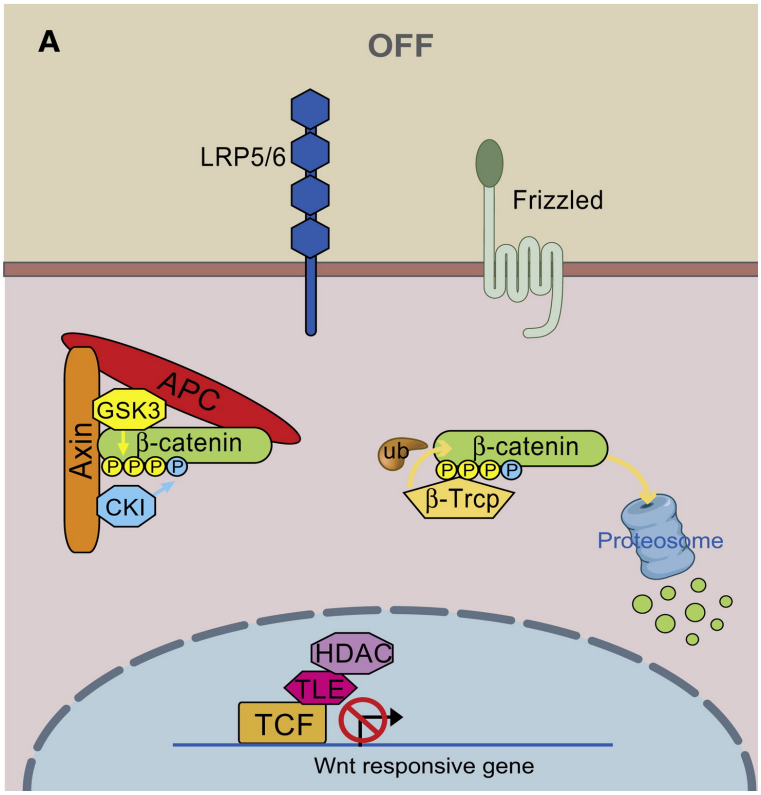

Figure 6. Overview of Wnt-off state

In the absence of Wnt, the serine threonine kinases, CKI and GSK-3β phosphorylate β-catenin.
β-catenin is recognized by β-Trcp, a component of E3 ubiquitine ligase complex.
Following ubiquitination, β-catenin is targeted to a rapid destruction by the proteasome.
In the nucleus, the transcription of Wnt target genes is inhibited by the corepressor protein Groucho/TLE (TLE) and histone deacetylases (HDAC).
Illustration by *Bryan T. MacDonald et al., Dev Cell. 2009 July; 17(1): 9-26.*

Several reports revealed that in colon adenocarcinoma and other type of cancers, missense mutation or deletion of presumptive GSK-3β phosphorylation sites in the β-catenin N terminus, make the protein resistant to regulation by the GSK-3β/APC/Axin complex [23,25,26]. The consequences of these mutations are: an increase in β-catenin cytoplasmic and nuclear levels, constitutive interaction of β-catenin with Tcf/Lef transcription factors, and activation of Tcf/LEF driven genes [23,27,28].

Contrariwise, on the **Wnt-on state** (Figure 7), Wnt ligand binds to a seven-pass transmembrane Frizzled (Fz) receptor and its co-receptor, *low-density lipoprotein receptor related protein 6* (LRP6) or its close relative LRP5 [23,29].

The formation of Wnt-Fz-LRP6 complex, together with the engagement of the scaffolding protein Dishevelled (Dvl), determines LRP6 activation by phosphorylation and the recruitment of Axin 1 to the receptor complex. These events lead to the inhibition of Axin-mediated β-catenin phosphorylation by CK1 and GSK-3β, causing β-catenin protein stabilization. Therefore, β-catenin moves into the nucleus to form complexes with Tcf/Lef proteins that enable the expression of Wnt-targeted genes responsible for cell growth and impairment of the apoptotic program (e.g *c-myc* oncogene).

From literature it is also known that nuclear accumulation of β-catenin impairs the transcription of the tumor suppressor gene *CDKN2A*, which encodes a protein ($p16^{INK4a}$) endowed with an inhibitory function on cell cycle progression [23,30].

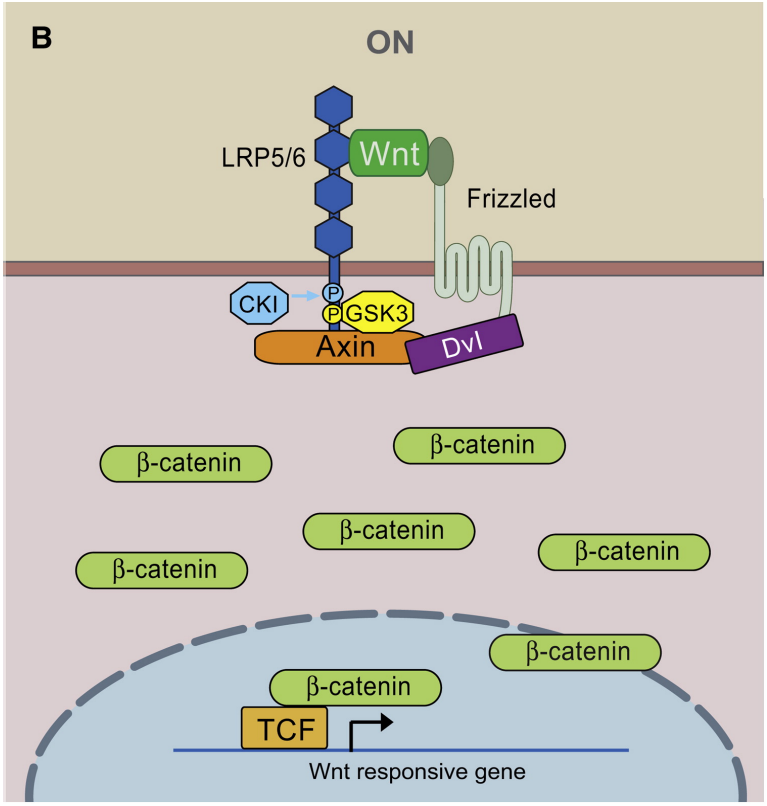

Figure 7. Overview of Wnt-on state

In the presence of Wnt ligand, the Fz/LRP5/6 co-receptor complex activates the canonical signaling pathways.
Fz interacts with Dsh and induce the recruitment of Axin.
The recruitment of Axin away from the "destruction" complex leads to the stabilization of β-catenin.
In the nucleus, β-catenin interacts with Tcf/Lef to promote the transcription of Wnt targeted genes.
Illustration by *Bryan T. MacDonald et al., Dev Cell. 2009 July; 17(1): 9-26.*

As regards CML, several studies indicated that deregulation of the Wnt/β-catenin axis occurs during the progression of the disease from chronic to accelerate and, finally, to blast crisis phases. It is well known, indeed, that normal hematopoietic stem cells (HSCs) self-renewal is sustained by β-catenin function but, on the pathological side, also CML progression towards the blast crisis seems to be consequent to the activation of β-catenin in GMP, in which it supports self-renewal and leukeamogenesis [14,17,18]. Although Wnt is the physiological trigger of β-catenin, BCR-ABL is able to sustain this activation, even independently of Wnt, by means of phosphorylation of β-catenin on tyrosine residues (Y86 and Y654) (Figure 8). Furthermore, as established in recent studies, BCR-ABL inhibits, by an Akt-dependent phosphorylation, the *glycogen synthase kinase 3β* (GSK-3β), a key regulator of β-catenin ubiquitination and proteasomal degradation (Figure 6)[19]. The serine/threonine kinase GSK-3β is indeed pivotal in multiple cellular processes including nutrient and energy homeostasis, proliferation and apoptosis, cell fate specification and stem cell self-renewal. As such, GSK-3β plays an essential role also linking the canonical Wnt pathway with the PI3K/Akt axis [17,19,20]. These findings suggest that β-catenin is likely to be an "hot-spot" for targeting LSCs self-renewal also in CML patients and therefore, to establish new treatments protocols in association with TKIs. However it should be noted that genetic deletion of β-catenin after CML initiation, does not lead to a complete remission of the disease, suggesting that other factors may sustain the progression of CML.

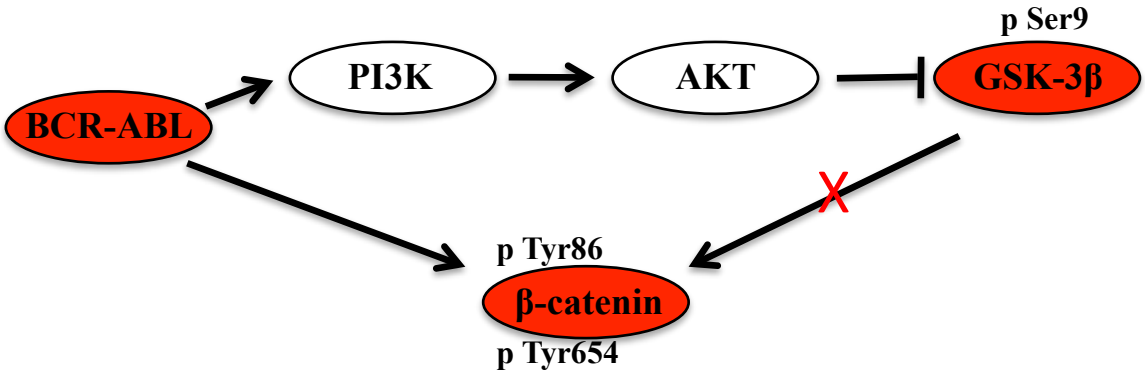

Figure 8. Schematic representation of β-catenin activation induced by BCR-ABL

1.4 Mammalian target of Rapamycin (mTOR) signaling pathway

Adding to its function in canonical Wnt/β-catenin signaling, previous works demonstrated that GSK-3β phosphorylates and activates the *tuberous sclerosis 2* (TSC2) protein, which possesses a GTPase-activating function [20,31,32]. Active TSC2, in turn, repress Rheb (*Ras homolog enriched in brain*), the small G-protein indispensable for the activation of *mammalian target of rapamycin-complex 1* (mTORC1) [20,33,34]. The *Mammalian target of rapamycin* (mTOR), contained in this protein complex, is an evolutionarily conserved serine/threonine kinase that regulates several cellular processes such as cell growth, cell cycle, cell survival and autophagy (Figure 9)[35,36]. Adding to this, recent reports indicate that mTOR drives also stem cell proliferation and self-renewal, and, more specifically, in BCR-ABL transformed cells [20].

More in general, mTOR takes can be recruited in two different protein complexes, mTORC1 and mTORC2 (Figure 9). mTORC1, comprises also proteins such as Raptor (*regulatory associated protein of mTOR*), mLST8 (*GβL, mammalian lethal with sec13 protein 8*), PRAS40 (*proline-rich Akt substrate of 40 kDa*) and Deptor. This complex is directly regulated by cellular energy and nutrient levels, plays an essential role in the regulation of translation and is sensitive to inhibition by rapamycin. The small GTPase Rheb, the key upstream activator of mTORC1, is negatively regulated by TSC2. Physiologically, mTORC1 is activated by growth factors downstream of PI3K and Ras signaling pathways, through the direct phosphorylation and inactivation of TSC2 that relies on the activity of Akt and other kinases (*extracellular signaling regulated kinase*, ERK, *p90 ribosomal protein S6 kinase*, RSK). However, when growth factor stimulation is withdrawn, TSC2-dependent inhibition of mTORC1 causes the cell to engage autophagy as an emergency response. Moreover, also a breakdown in energy supply negatively regulates mTORC1 formation consequently to the phosphorylation of Raptor by the *AMP-activated protein kinase* (AMPK).

The signaling downstream of mTORC1 mainly implies the phosphorylation and activation of *p70 ribosomal S6 kinase 1* (S6K1) and *eukaryotic initiation factor 4E-binding protein 1* (4E-BP1), likely to be recruited by Raptor that acts as a scaffolding protein (Figure 9)[34,35,36]. mTORC1-dependent phosphorylation of S6K1 (on threonine 389), is required to recruit the *phosphoinositide-dependent-kinase*-1 (PDK1) and to stimulate mRNA processing, protein synthesis and cell growth. On the other hand, 4E-BP1, which is a member of the 4EBP family having a repressive function on translation initiation, dissociates from eIF4E upon mTORC1-dependent phosphorylation, thus enabling progression of protein synthesis. Recent studies also demonstrate that 4E-BP1 is a crucial element of the mTORC1 pathway affecting cell number and proliferation [36].

The alternative complex, mTORC2, consists includes Rictor (*rapamycin-insensitive companion of mTOR*), mSin1 (*mammalian stress-activated mitogen-activated protein kinase-interacting protein 1*), PRR5 (*proline-rich region 5*), mLST8 and Deptor (Figure 9).

This complex is not directly influenced by cellular energy and nutrient levels and it is insensitive to inhibition by rapamicyn. Biochemical and genetic evidence is provided that

mTORC2 phosphorylates Akt at serine 473, creating a mechanism of resistance to pro-apoptotic stimuli [35,36] (Figure 9).

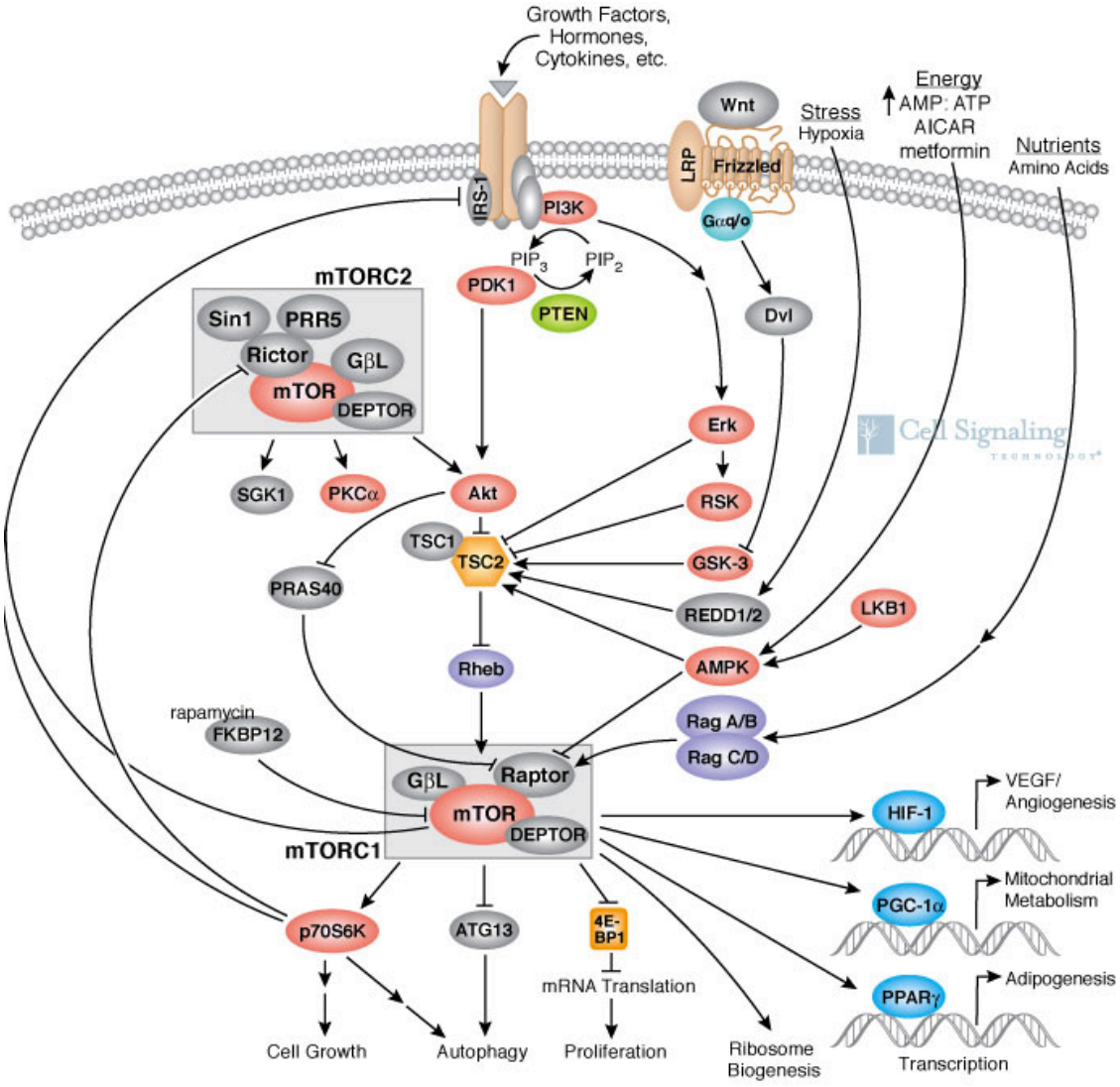

Figure 9. Overview of mTOR signaling pathway

mTOR is an evolutionarily conserved serine/threonine protein kinase that regulates several cellular processes such as cell growth, cell cycle, cell survival and autophagy; it is charactherized by two functional complexes mTORC1 and mTORC2. mTORC1 is directly regulated by cellular energy and nutrient status, plays an essential role in the regulation of translation and autophagy and is sensitive to inibhition by rapamycin. Instead, mTORC2 is not directly regulated by cellular energy and nutrient status, is insensitive to inhibition by rapamicyn and phosphorylates Akt at serine 473, therby contributing to growth factor-mediated Akt activation.
Illustration by *Cell Signaling Thecnologies Pathways web site (www.cellsignaling.com).*

1.5 AMPK signaling pathway

As already stated, under metabolic stress conditions, mTORC1 activity is inhibited by AMPK. It has been shown that AMPK inhibits mTORC1 by two different mechanisms: one through the activation of TSC2, which promotes the inhibition of Rheb, and the other through direct phosphorylation of Raptor at serine 792 (Figure 11) [36,40].

AMPK is a highly conserved serine/threonine protein kinase, found in all eukaryotes, member of the AMPK-related kinase family [36,37,38], which works as metabolic sensor to govern glucose and lipid metabolism in response to alteration in nutrients and intracellular energy levels. AMPK is a hetero-trimer comprising the catalytic α subunit and two other subunits, β and γ, with regulatory function. In mammals, each subunit has multiple subtypes; in particular, there are two isoforms of the catalytic subunit α (α1 and α2), while β and γ subunits have respectively two (β1 and β2) and three isoforms (γ1, γ2, γ3). The β subunit functions as a scaffold, that brings together α and γ subunits. The γ subunit contains four repeats of the *cystathionine beta synthase* (CBS) homology domains conferring the ability to bind molecules with adenosyl groups, i.e. AMP, ADP and ATP (Figure 10)[38].

This kinase AMPK is activated by phosphorylation of the threonine 172 residue located in the activation loop of the α subunit, an event that is catalyzed by upstream kinases, such as *liver kinase B1* (LKB1) and *Ca^{2+}/Calmodulin-dependent protein kinase kinase-β* (CaMKK-β) (Figure 10). While CaMKK-β-dependent activation of AMPK is under control of intracellular Ca^{2+} currents [36,39], the tumor suppressor LKB1 activates AMPK in response to a decline of ATP levels as occurs upon nutrient starvation, ischemia and hypoxia. Under these conditions, active AMPK phosphorylates many substrates to turn on catabolic pathways, in order to generate more ATP, and to turn off those processes that are energy demandings [36,38].

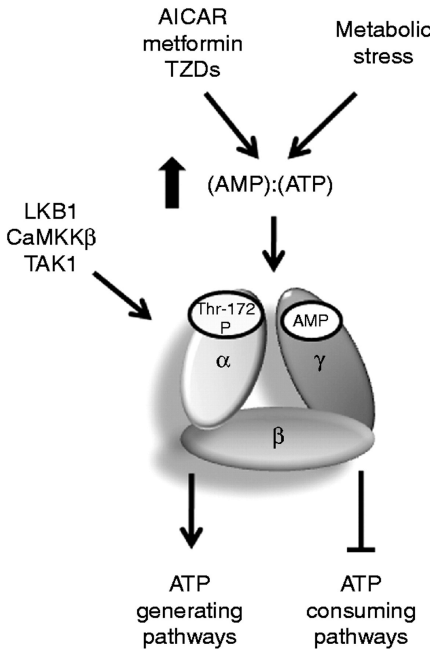

Figure 10. Structure and regulation of AMPK

AMPK is a heterotrimeric protein consisting of three different subunits: α, with catalytic function, and β and γ, which are regulatory of AMPK catalysis. AMP binding to the regulatory γ subunit of AMPK promotes the phosphorylation and activation of the α subunit (on threonine 172) by the upstream kinase LKB1. Alternatively, this kinase is activated by CaMKK-β in response to intracellular Ca^{2+} currents.
Illustration by *J Jeyabalan, et al., Journal of Endocrinology, 2012; 212: 277–290.*

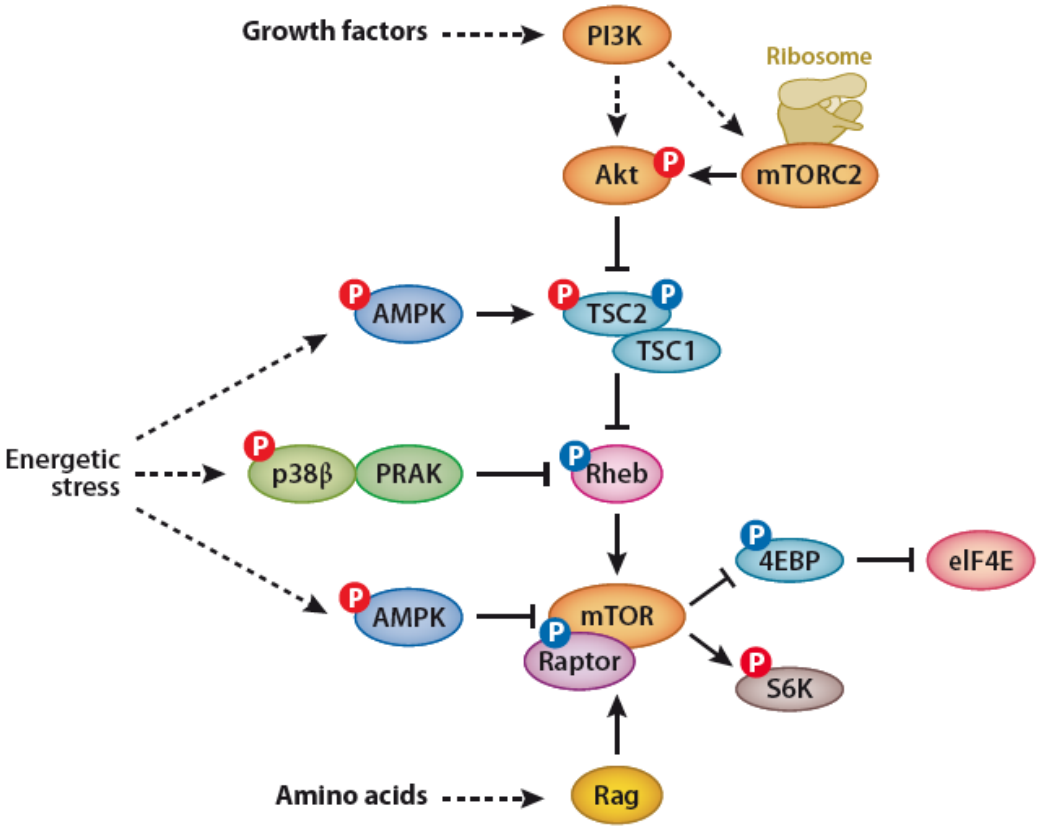

Figure 11. Regulation of mTORC1 by AMPK

AMPK inhibits the pathway of mTORC1 in multiple mechanisms. Under energetic stress condition, AMPK phosphorylates TSC2 and Raptor to inhibit the mTORC1 complex.
Illustration by *Ken Inoki et.al., Annu. Rev. Pharmacol. Toxicol. 2012;52:381-400.*

Recently, several works demonstrated that pharmacological activators of AMPK, such as metformin and 5-aminoimidazole-4-carboxamide ribonucleotide (AICAR), suppress the activation of mTORC1 pathway in BCR-ABL positive cells. Strikingly, treatments with these compounds induce a potent suppression of cell proliferation in Ph^+ CML and acute lymphoblastic leukaemia (ALL) models, including cells expressing the T315I mutant of BCR-ABL [(40,41)].

1.6 Autophagy

Macroautophagy (hereafter named autophagy) is a degradation process that, under homeostatic conditions or in response to stress signals, consists in the lysosomal break down of intracellular material to enable cell adaptation to developmental and environmental signals [(42,44)].

Autophagy is evolutionarily conserved and, in eukaryotes, progresses through delineate steps for the encapsulation of long-lived proteins and unbroken organelles into double membrane vesicles named autophagosomes. Finally, autophagosomes fuse with lysosomes to form autophagolysosomes, in which lysosomal hydrolases digest the vesicle for final destruction and recycling [(42,43)].

In more details, the formation of autophagosomes is a three step-process characterized by nucleation, elongation, and completion of an isolation membrane, or phagophore. This process is strongly regulated by a limited number of highly conserved genes called autophagy regulators (ATGs) (Figure 12)[(42,44,45)].

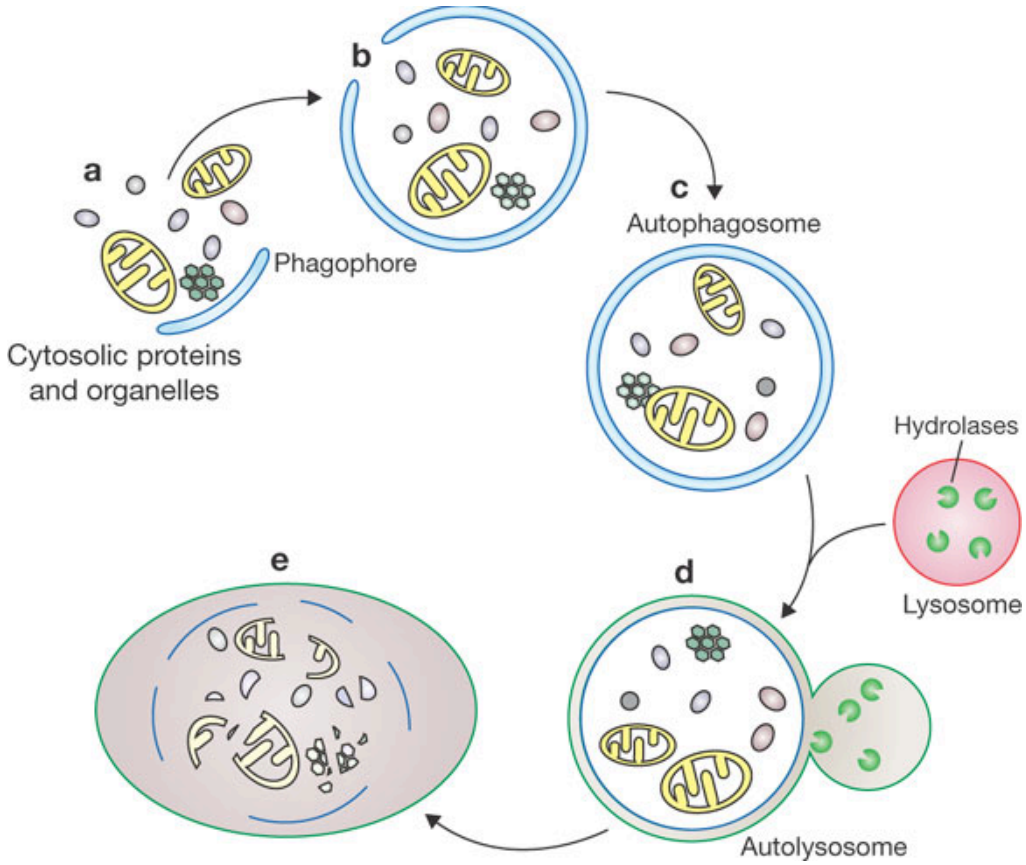

Figure 12. Schematic diagram of the steps of autophagy

Autophagy begins with the formation of the phagophore or isolation membrane. The concerted action of the autophagy core machinery proteins at the phagophore assembly site is thought to lead to the expansion of the phagophore into an autophagosome. The autophagosome can engulf bulky cytosolic material, including entire organelles. When the outer membrane of the autophagosome fuses with an endosome or directly with a lysosome, it forms an autophagolysosome. Finally, the sequestered material is degraded inside the autophagolyosome and recycled.

Illustration by *Zhiping Xie, Daniel J. Klionsky, Nature Cell Biology, 2007; 9:1102 –1109.*

By allowing metabolic adaptation of the cell to multiple stresses, such as a decrease in nutrients, alterations of the oxidative metabolism, hypoxia, engulfment of endoplasmic reticulum and viral infections, autophagy provides an escape form apoptotic death (programmed cell death). However, depending on the duration and/or the intensity of the initial stress, autophagic cells may engage a specific cell death program called "autophagic cell death" (ACD) or type II cell death [44,46].

Autophagy is found activated also in cancer cells in which it may promote cancerogenesis. On the other hand, evidence has been provided that autophagy can sometime increase apoptosis of cancer cells, thus expressing a tumor-suppressor function. Hence the precise role of autophagy during cancer progression is thought to be both tissue and context dependent [45,47].

Another interesting aspect of autophagy is its involvement in the response to chemotherapy and radiation. Most of the studies indicate that autophagy inhibition sensitizes tumor cells to cell death induced by irradiation, alkylating agents or arsenic trioxide, suggesting that cancer cells can react to chemotherapy by inducing autophagy as a self-defense mechanism. Following anti-cancer treatments, the high levels of autophagy observed in tumor cells commonly represent an adaptive response that enables survival. In line with this assumption, several works demonstrated that autophagy inhibition synergizes with chemotherapies underlining the possibility that, the pharmacological inhibition of autophagy may represent an adjuvant therapy for cancer [44,45,47].

For instance, synergism between pharmacological inhibitor of autophagy and common chemotherapies has been confirmed by treating several type of cancer (glioma, multiple myeloma, breast, colon and prostate cancer), including CML. In the latter case, it was demonstrated that resistance to TKIs might in part rely on massive engagement of autophagy, providing the rational for inhibiting this process in view of a therapeutic response. Indeed, recent works demonstrates that imatinib-dependent inhibition of BCR-ABL may cause the activation of autophagy, which is consequent to alterations in intracellular Ca^{2+} concentrations and ER stress. Thus, combination of imatinib and chloroquine, an inhibitor of the final step of autophagy (digestion of cytosolic material in the autophagolysosome), significantly augments cell death of CML blasts, independently of the stage of the disease. In support, similar results were obtained abrogating the expression (by means of RNA-interference) of essential autophagy genes (atg5, atg7). More importantly, it has been proved that LSCs (identified as the $CD34^{+}/CD38^{-}$ subpopulation of leukaemic blasts) are intrinsically resistant to imatinib by virtue of efficient engagement of autophagy, reinforcing the clinical implication of treatments that impair this process [6,44,47]. In agreement, also vorinostat (an HDAC inhibitor) was found synergetic with chloroquine in killing imatinib-refractory CML cells [45,47], suggesting a more general impact of autophagy inhibition on cancer therapy.

All these studies were used in support of the first clinical trial that propose the inhibition of autophagy in the treatment of CML patients, named CHOICES ("Chlroquine and Imatinib Combination to Eliminate Stem cells"), which is currently on phase II [6,47].

1.7 Celecoxib and 2,5-Dimethylcelecoxib

Celecoxib is a sulfonamide non-steroidal anti-inflammatory drug (NSAID) and a selective cyclooxygenase-2 inhibitor (COXIB) used in the treatment of osteoarthritis and rheumatoid arthritis (Figure 13). Beyond its use as anti-inflammatory drug, celecoxib is known to exert an anti-proliferative control in many models of solid tumours. In particular, it is the only NSAID that has been approved for adjuvant treatment of patient with familial adenomatous polyposis. However, the antitumor activity of celecoxib in hematopoietic tumors, especially in CML, has not established so far [48,49].
Celecoxib is able to inhibit both cyclooxygenases 1 (COX-1) and 2 (COX-2), although it is 10-20 times more selective towards the latter isoenzyme.

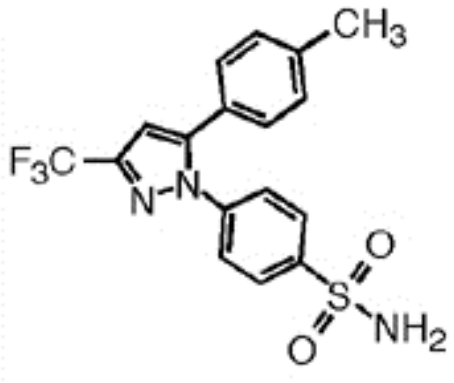

Figure 13. Chemical structure of celecoxib

Illustration by *Schönthal AH, British Journal of Cancer, 2007; 97, 1465-1468.*

COXs are the key enzymes that catalyze the conversion of arachidonic acid to prostaglandins and other eicosanoids. In most tissues, COX-1 is expressed constitutively, whereas growth factors, cytokines and carcinogens may induce the expression of COX-2. Strikingly, high levels of PGE_2 associated to an over-expression of COX-2 have been documented in several malignancies of colon, breast, prostate, pancreas and skin [50].
Such over-expression of COX-2 in tumor cells is suggested to generate several cancer-promoting effects, e.g. the over-expression of pro-angiogenic factors (VEGF, IL6, IL8), the activation of metalloproteases (MMP1, MMP2) and resistance to apoptosis inducing stimuli. The underlying mechanism proposed to explain some of the pro-survival effects of COX-2 hyperactivity is the increased conversion of arachidonic acid to PGE_2 that, through the engagement of EP (1, 2, 3 and 4) class of g protein-coupled receptors (GPCR), causes cellular responses. For instance, acting on EP2 and 3 receptors of the cancer cell, PGE_2 is entitled to sustain proliferation, consequent to impairment of the p27 CDK inhibitor, and, at the same time, to inhibit apoptosis through an up-regulation of Bcl-2 [51]. Moreover, PGE_2 may exert its cancerogenic potential at the level of the immune system, where it co-operates with macrophages to provide a “tumor supportive” microenvironment [50,52].
Nevertheless, there are an increasing number of reports indicating that celecoxib does not require the presence of COX-2 in order to exert its antitumor activities. The hypothesis of COX-2-independent effects are based on the evidence that celecoxib exerts its anti-proliferative and pro-apoptotic function also in cancer cell lines that do not express COX-2

[53,54]. In line with those findings, it was also demonstrated that 2,5-dimethylcelecoxib (DMC), a close structural analogue of celecoxib devoid of COX-2 activity, is able to potently mimic all antitumor proprieties of celecoxib (Figure 14)[55,56,57].

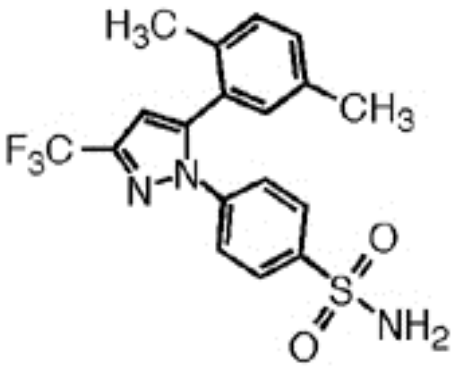

Figure 14. Chemical structure of 2,5-dimethylcelecoxibcelecoxib

Illustration by *Schönthal AH, British Journal of Cancer, 2007; 97, 1465-1468.*

To this regard, recent reports have proposed some molecular targets alternative to COX-2, such as: PDK1 (Phosphoinositide-Dependent Kinase-1), SERCA (Sarco/Endoplasmatic Reticulum Ca^{2+}ATPase), carbonic anhydrase, and 5-lipoxygenase (ALOX5)[48,57,58]. Finally, more recent studies on human colon carcinoma models have identified in β-catenin and its underlying pathway a possible target for COX-2-idependent action of celecoxib [59].

Thus, in absence of a functional COX-2 enzyme, it is of great importance to evaluate the potential involvement non-COX-2 targets, already proposed or yet to be identified, in order to propose and optimize the use of celecoxib in the treatment of responsive cancers [55,60,61].

Chapter 2:

Materials and Methods

2. Materials and Methods

2.1 Cell Cultures

The BCR-ABL positive, human CML cell lines K562, LAMA-84 and JURL-MK1, which are provided by the American Type Culture Collection (ATCC, Rockville, MD, USA), have been established form the peripheral blood of three different patients during the blast crisis stage of the disease. Cell lines were grown in suspension in presence of Roswell Park Memorial Institute medium (RPMI-1640*;* Sigma-Aldrich Inc., Milan, Italy) supplemented with 10% heat-inactivated fetal bovine serum (FBS, Immunological sciences, Rome, Italy), l-glutamine 50 mg/mL (Sigma-Aldrich Inc., Milan, Italy), penicillin 10 U/mL and streptomycin 100 mg/mL (Sigma-Aldrich Inc., Milan, Italy).
The cell line expressing the β-catenin S33Y mutant was obtained by gene transfection (see further in the text) and it was maintained in a RPMI-1640-based medium, as described for the parental cell line LAMA-84.
AMPKα-silenced cells, AMPKα$^-$, and their un-targeted counterpart, SCR, were obtained by lentiviral delivery of microRNAs (see further in the text), and were cultured as the originator cell line, LAMA-84.
HeLa cells were obtained from ATCC (Rockville, MD, USA) and were cultured in Modified Eagle's Medium (MEM*;* Sigma-Aldrich Inc., Milan, Italy), supplemented with 10% heat-inactivated FBS (Immunological sciences, Rome, Italy), l-glutamine 50 mg/mL (Sigma-Aldrich Inc., Milan, Italy), penicillin 10 U/mL and streptomycin 100 mg/mL (Sigma-Aldrich Inc., Milan, Italy).
All cell lines were kept in culture at 37 °C, under a 5% CO_2 humidified atmosphere.

2.2 Chemicals

Celecoxib (4-[5-(4-methylphenyl)-3-(trifluoromethyl)-1H-pyrazol-1-yl]benzenesulfonamide, 200 mM stock solution; Chemos GmbH, Regenstauf, Germany); rofecoxib (3-(4-methylsulfonylphenyl)-4-phenyl-2H-furan-5-one, 50 mM stock solution; MSD Inc., Milan, Italy); MG132 (Z-Leu-Leu-Leu, 50 mM stock solution), BIO (10 mM stock solution), STO-609 (10 mg/mL stock solution), all purchased from Sigma-Aldrich Inc., Milan, Italy; PP242 (50 mM stock solution; Selleck Chemicals, Munich, Germany); imatinib (4-[(4-methylpiperazin-1-yl)methyl]-N-[4-methyl-3-[(4-pyridin-3-ylpyrimidin-2yl)amino]phenyl]benzamide; 50 mM stock solution; LKT Laboratories Inc., St. Paul, MN, USA); these compounds were dissolved in 100% dimethyl sulfoxide (DMSO) and stored at +4 or -20°C, according to manufacturers' specifications. Working concentrations of

these compounds were freshly prepared for each experiment by diluting DMSO to 0.1% in milliQ (MilliPore) water.
A 100 mM stock solution of chloroquine (Sigma-Aldrich Inc., Milan, Italy) was obtained by diluting it in milliQ water (MilliPore) and stored at -20°C.
2,5-dimethyl-celecoxib (4-[5-(2,5-dimethylphenyl)-3-(tryfluoromethyl)-1H-pyrazol-1-yl]benzenesulfonamide, 100 mM stock solution; WITEGA Laboratorien GmbH, Berlin, Germany) was synthesized as follows by Dott. Minassi (Department of Pharmaceutical Sciences, Novara, Italy).

2.3 3-(4,5-Dimethylthiazol-2-Yl)-2,5-Diphenyltetrazolium Bromide (MTT) assay

Cells were plated in 96-well plates (100 μL/well) and treated at a 5-10x10^4cells/mL density. At the end of the treatments, the MTT reagent was added to cells at a final concentration of 0,25 mg/mL (Sigma-Aldrich Inc., Milan, Italy), for 90 minutes at 37°C. Reactions were then stopped and the crystal were solubilized by adding isopropyl alcohol/HCl (1:1; vol:vol) (Sigma-Aldrich Inc., Milan, Italy) plus 10% Triton X-100 (Sigma-Aldrich Inc., Milan, Italy), before reading the absorbance at 570 nm, using the multi-plate reader Victor3 V (PerkinElmer, Milan, Italy).

2.4 Analysis of Cell Cycle distribution by Flow Cytometry

At the end of the various treatments, 1x10^6 cells were collected, washed once with Phosphate Buffer Saline (PBS) and resuspended in a 70% ethanol solution. Following to overnight incubation at -20°C, cells were washed again with PBS and incubated with RNAase (100 μg/mL, Sigma-Aldrich Inc., Milan, Italy). Cells were then incubated in PBS containing 5 mM EDTA and 50 μg/mL propidium iodide (Sigma-Aldrich Inc., Milan, Italy) for 30 minutes, prior to flow cytometric analysis with Accuri-C6 flow cytometer (BD Bioscience, Milan, Italy). ModFit LT software was used for discrimination of different sub-populations along the cell-cycle.

2.5 Staining of apoptotic nuclei

Nuclear DNA integrity was assessed through microscopy of cells stained with the DNA-binding, supravital dye, Hoechst-33342 (Sigma-Aldrich Inc., Milan, Italy).
Briefly, cell were incubated with 0.8 μg/mL Hoechst-33342 for 15 minutes at room temperature prior to fixation with 4% PBS/paraformaldehyde (Sigma-Aldrich Inc., Milan,

Italy), for 10 min at room temperature. Cells were then washed twice with PBS, spotted on a microscope slide by cyto-spinning (10 minutes x 1200 rpm) (Thermo Fisher Scientific Inc., Milan, Italy) and layered with mounting solution (DakoCytomation Carpinteria, CA, USA) and cover slip. Images (60x magnification, Nikon Instruments, Florence, Italy) were obtained through UV-excitation of the samples and documented with a digital camera (Nikon Instruments, Florence, Italy).

2.6 Clonogenic Assay

Cells were treated, for 24 hours at the $1x10^5$cells/mL density, with the concentrations indicated for each drug (celecoxib, dimethyl-celecoxib, rofecoxib, PP242, STO-609, chloroquine and imatinib), or with vehicle (0.1% DMSO). Next, 1250 cells/well (in 6-well plates) were seeded into a semisolid culture media composed of 80% methylcellulose (MethoCult®, STEMCELL Tech., Milan, Italy) and 20% RPMI-1640 (fully supplemented). After 6 days, cell colonies were counted using a phase-contrast microscope.

2.7 Immunoblottings

Whole-cell extracts were obtained using the RIPA lysis buffer (50 mM Tris-HCl pH 7.4; 150 mM NaCl, 0.5 mM EDTA pH 8, 1% Igepal, 0.1% SDS), supplemented with 1 mM phenylmethylsulphonyl fluoride, 1 mM sodium orthovanadate, 50 mM sodium fluoride, 10 mM glycerophosphate, 0.5 mM dithiothreitol and standard protease inhibitor cocktail (Roche Applied Science, Indianapolis, IN, USA).
Lysates were clarified by centrifugation at 14000g for 15 minutes at 4°C. Protein concentrations were evaluated with Bradford reagent (Sigma-Aldrich Inc., Milan, Italy).
For LC3 protein detection, cell extracts were obtained directly in 2xLaemmli sample buffer, supplemented with β-mercaptoethanol (Sigma-Aldrich Inc., Milan, Italy).
Proteins were loaded onto SDS-PAGE gels for electrophoresis, and transferred onto 0.22μ nitrocellulose or PVDF membranes for immunodetection.
The following primary antibodies were used: anti β-actin (clone AC-15 Sigma-Aldrich Inc., Milan, Italy); anti-COX-1 (clone H-62, Santa Cruz Biotechnology Inc., Santa Cruz, CA, USA); anti-COX-2 (clone C-20, Santa Cruz Biotechnology Inc., Santa Cruz, CA, USA); anti-β-catenin (clone 14, BD Bioscience, Milan, Italy); anti-non-phospho(active)-β-catenin (ser33/37/thr41, Cell Signaling Technology Inc., Danvers, MA, USA); anti-phospho-AMPKα (thr172 clone 40H9) and AMPK-α (Cell Signaling Technology Inc., Danvers, MA, USA); anti-phospho-GSK-3β (ser9) and anti-GSK-3β (Cell Signaling Technology Inc., Danvers, MA, USA); anti-phospho-mTOR (Ser2448), anti-phospho-mTOR (ser2481) and mTOR (clone 7C10) (Cell Signaling Technology Inc., Danvers, MA, USA); anti-phospho-

p70 S6 Kinase (thr389) and anti-p70 S6 Kinase (Cell Signaling Technology Inc., Danvers, MA, USA); anti-phospho-4E-BP1 (thr37/46) and anti-4E-BP1 (Cell Signaling Technology Inc., Danvers, MA, USA); anti-LC3B (Sigma-Aldrich Inc., Milan, Italy).
Antibodies were all prepared in TRIS-buffered saline solution containing with 0.1% Tween-20 (T-TBS), and supplemented with 3-5% non-fat dried milk or 3-5% bovine serum albumin, depending on the indications of the manufacturers.
After over-night incubation at 4°C, membranes were washed trice in T-TBS and incubated (45 minutes at room temperature) with appropriate horseradish peroxidase-conjugate secondary antibody (Bio-Rad Inc., Milan, Italy), before visualization of the chemiluminescent substrate PDS-OVERTIME (Genespin, Milan, Italy). Images of the immunoreactive bands were acquired and analyzed using the ChemiDoc XRS device (Bio-Rad Inc., Milan, Italy) and the Quantity-One software (Bio-Rad Inc., Milan, Italy).

2.8 RNA extraction, reverse transcription and quantitative Real-Time PCR (qRT-PCR)

Total RNA was extracted approximately from 5 x10^6 cells using TRI-Reagent® (Sigma Aldrich Inc., Milan, Italy). Im-Prom-II™ Reverse Transcriptase (Im-Prom-II™ Reverse Transcription System, Promega, WI, USA) was used to generate cDNA using 1 μg of RNA and oligo dT primers, according to the instructions of the manufacturer. Reverse transcription was performed using a thermal-cycler (Eppendorf, Germany) and the following heating protocol: 10 minutes at 25°C, 45 minutes at 42°C and 5 minutes at 99°C. cDNA was then stored at -20°C until further used.
After setting gradient PCRs to verify primers specificity and melting temperature, standard curves of SYBR Green fluorescence were generated for each gene tested in order to evaluate primer efficiency.
qRT-PCRs were performed on a 96-well plate, in triplicate, and florescence intensity assessed using the CFX96™ Real-Time PCR Detection Systems (Bio-Rad Inc., Milan, Italy). The following conditions were adopted: 12.5 μL Maxima™ SYBR Green/ROX qPCR Master Mix (Thermo Fisher Scientific Inc., Milan, Italy), 0,1 μM of forward and reverse primers, and 5 μL of 1:5 diluted cDNA, in a total volume of 25 μL/reaction.
After an initial denaturation step at 95°C (10 minutes), each primer set was used (through 40 cycles of amplification) as follows: human *CTNNB1*, 5'-ACCAGCGCCGTACGTCCAT-3' forward and 3'-GCTAGGATGTGAAGGGCTCCG-5' reverse (104-bp amplicon) (Sigma-Aldrich Inc., Milan, Italy), 60°C annealing temperature; human *c-myc*, 5'-CAAAGACAGCGGCAGCCC-3' forward and 3'-GCGAGGCGCAGGACTTG-5' reverse (164-bp amplicon) (Sigma-Aldrich Inc., Milan, Italy), 64.4°C annealing temperature; human *CDKN2A*, 5'-CAACCTGGGGCGACTTCAG-3' forward and 3'-GACCAGCCAGCCCCTCC-5' reverse (201-bp amplicon) (Sigma-Aldrich Inc., Milan, Italy), 61.7°C annealing temperature.

CTNNB1, *c-myc* and *CDKN2A* transcripts were normalized to the expression of glyceraldehyde-3-phosphate dehydrogenase (GAPDH) mRNAs, assessed using the 5'-CAAGGTCATCCATGACAACTTTG-3' forward and the 3'-GGGCAATCCACAGTCTTCTG-5' reverse primer (90-bp amplicon) (Sigma-Aldrich Inc., Milan, Italy), 60°C annealing temperature.
At the end of the amplification cycles, amplicon/primers melting curves were generated measuring the SYBR Green fluorescence upon temperature ramping from 60°C to 95°C (0.3°C/s). For each gene, the threshold cycle (C_t) was calculated using CFX Manager Software (Bio-Rad Inc., Milan, Italy) by determining the cycle number at which the change in the fluorescence of the reporter dye crossed the threshold. The C_t of treated cells was compared to the C_t generated by the control cells and ΔC_t was calculated as the difference between C_t values, determined using the equation $2^{-\Delta Ct}$.

2.9 Constructs, transfection, lentiviral infection

LAMA-84 β-catenin S33Y cells were obtained by stable transfection of a pcDNA3 plasmid carrying the cDNA for a Flag-tagged degradation-resistant mutant of β-catenin in which serine 33 has been replaced by a tyrosine (Addgene, Cambridge, MA, USA).
Transfection was performed by using the X-tremeGENE reagent (Roche, Milan, Italy), according to the indications of the manufacturer. After 24 hours from transfection, cells were exposed for 10 days to the selecting agent G418 (0,8 mg/mL; Sigma Aldrich Inc., Milan, Italy). The expression of the exogenous protein (S33Y β-catenin) was verified by immunoblots with the anti-Flag rabbit polyclonal antibody (Sigma Aldrich Inc., Milan, Italy).
To knock-down of the AMPKα kinase, pGIPZ vectors carrying the non-targeting (SCR) or nine different AMPKα-specific (AMPKα$^-$) miRNAs (all obtained through access to the Open Biosystems library, at the Cancer Institute, University College of London) were screened in preliminary experiment by using the immunoblotting technique.
Lentiviral supernatants were prepared, following to the manufacturer's instructions, using the HEK-293T cell lines for virus packaging. Cell were transfected with a mix (4:3:1) of pGIPZ (carrying miRNA sequence and the reporter gene turbo-Green Fluorescence Protein, tGFP), psPAX2 (carrying the HIV-derived *gag/pol*, *rev* and *tat* sequences) and pMD2.G plasmids (coding for the *env* protein of the *Vesicular Stomatitis Virus G*, required for virion pseudotyping) using the METAFECTENE® PRO reagent (Biontex Laboratories GmbH, Germany).
Lentiviral particles were concentrated after two centrifugation steps (1.500 g, 4°C) in a solution containing polyethylene glycol (PEG MW8,000, Sigma Aldrich Inc., Milan, Italy) and then re-suspended in PBS (1/50 of the initial volume).
Titration was performed on HeLa cells infected with (1:5) serial dilutions of the viral suspension. Infection efficiency was calculated by assessing, through flow cytometry, percentages of cells expressing the tGFP reporter gene contained in the pGIPZ plasmid.

The infections were carried out by *spinoculation* procedure. Briefly, $1x10^6$ cells/mL, plated in 6-well plates, were exposed to viruses at a concentration of 10 multiplicity of infection (MOI) in presence of 8µg/mL of Polybrene® (Sigma Aldrich Inc., Milan, Italy). Incubation with viruses was allowed upon centrifugation for 45 minutes at 1260rpm; next, cells were incubated for 5 hours at 37°C before being switched to regular medium.
Green fluorescence intensity was used as reference parameter in order sort out (using the FACS-Vantage cell sorter) the population of cells with the highest levels of viral integration. Finally, the down-regulation of AMPKα was verified by probing protein lysates with the anti-AMPKα rabbit polyclonal antibody (Cell Signaling Technology Inc., Danvers, MA, USA).

2.10 Immunofluorescence and Autophagy assessment

Following treatments with drugs (celecoxib and chloroquine), cells were fixed with 4% PBS/paraformaldehyde (Sigma Aldrich Inc., Milan, Italy) for 15 minutes at room temperature. Next, cell were washed three times with PBS and then permeabilized using 0,1% Triton X-100/PBS (Sigma-Aldrich Inc., Milan, Italy) for 10 minutes. After three washing steps, saturation of unspecific epitopes was achieved through incubation with the PBG buffer (0.5% bovine serum albumin, 0.2% gelatin from cold water fish skin in PBS; Sigma-Aldrich Inc., Milan, Italy) for 60 minutes at room temperature, before adding the rabbit anti-LC3B antibody (Sigma-Aldrich Inc., Milan, Italy), which was incubated for 90 minutes at room temperature. Finally, LC3-postive structures were visualized, after three washes with PBS, by incubation (for 30 minutes at room temperature) with an anti-rabbit secondary antibody conjugated with the fluorochrome Alexa-Fluor488 (Life Technologies Corporation, Milan, Italy). Nuclei were counter stained using Hoechst-33342 (Sigma-Aldrich Inc., Milan, Italy). Cells were then spotted on a microscope slide by cyto-spinning (10 minutes x 1200 rpm) (Thermo Fisher Scientific Inc., Milan, Italy) and layered with mounting solution (DakoCytomation Carpinteria, CA, USA) and cover slip. Images (60x or 100x magnifications) were acquired using an inverted microscope equipped with epi-fluorescence attachment and a digital camera (Nikon Instruments, Florence, Italy).
A minimum of 200 cells was counted for each treatment and replicated in three independent experiments. Autophagic cells were identified as those displaying at least four LC3-positive puncta.

2.11 Statistical Analysis

The results in this study are presented as mean (± standard error) of the results obtained from three independent experiments. Statistical analyses were performed using Student's t-test. Statistical significance was indicated as follows: *P<0.05 (*), P<0.01 (**), P<0.001 (***)*.

Chapter 3:

Results

3. Results

3.1 Celecoxib impairs proliferation of CML cell lines

To investigate the effects of celecoxib on CML viability we generated concentration-response curves in three p210-BCR-ABL-expressing CML cell lines (K562, LAMA-84, JURL-MK1), exposed to this drug for 24 hours using the MTT assay (Figure 15a). Proliferation inhibition, reflected by the ability of celecoxib to suppress cellular metabolism of the tetrazolium substrate used for this assay, was especially evident in the LAMA-84 cell line (EC50 of about 23,8 μM), while the JURL-MK1 was the most resistant of the three lines (EC50 of 75,2 μM). The impact of celecoxib on tetrazolium conversion was also irreversible and time-dependent since the EC50, calculated 6 days after a single administration of this drug, was consistently lower than at 24 hours (8,2 μM for LAMA-84 and 23,8 μM for JURL-MK1) (Figure 15b).

A careful analysis of the data also revealed that, after 24 hours, MTT absorbance of celecoxib-treated cells, although reduced in comparison to control groups (0,1 % DMSO, used as vehicle), did not reach levels below the time-zero point (unless using concentrations higher than 25 μM, Figure 15a), implying a cytostatic rather than a cytotoxic effect. Cell counting with a hemocytometer confirmed that numbers lower than those of time-zero were observed in the celecoxib-treated group only at concentrations higher than 25 μM (data not shown).

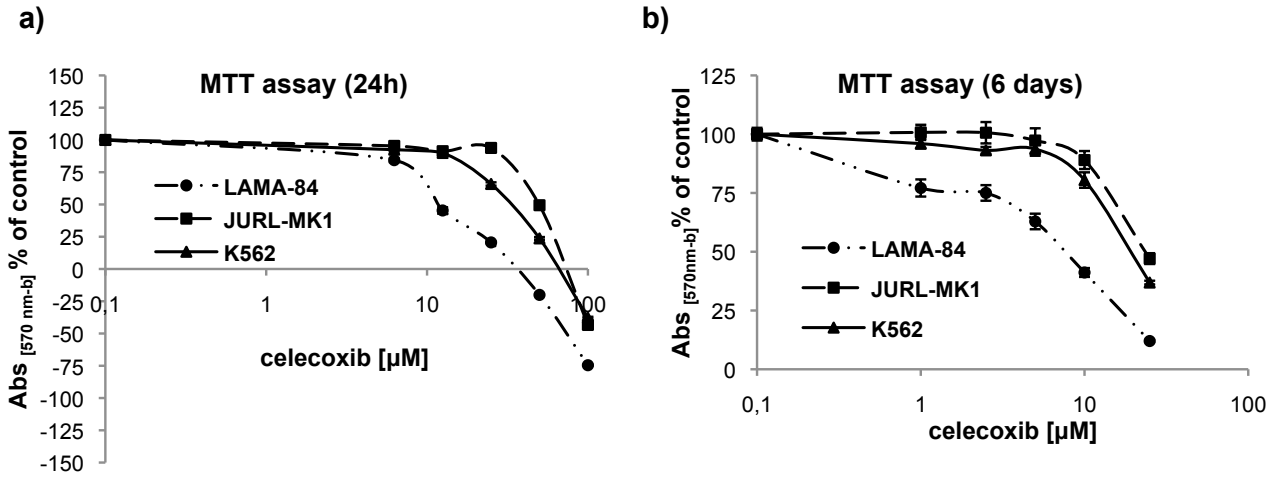

Figure 15. Cell viability, dose-response curves of LAMA-84, JURL-MK1 and K562 cell lines evaluated by MTT assay.

Cells were treated for: **a)** 24 hours with 6.25, 12.5, 25, 50, 100 μM celecoxib; **b)** or 6 days with 1, 2.5, 5, 10, 25 μM celecoxib. Data represents averages of three independent experiments (± standard error).

LAMA-84 cell cycle profiling, by means of flow cytometry of propidium iodide stained cells, evidenced that celecoxib, at concentrations close to the EC50 (25 μM), caused an increase in the apoptotic SubG1 peak (13,6 % vs 1,1% of controls) as well as in the G1 cell subset (61,8 % vs 55,2 % of controls); these variations were associated to a contemporary depletion of the S (20,6 % vs 28,6) and G2 (4 % vs 15,1%) subpopulations. Conversely, celecoxib had no effect on the cell cycle distribution of JURL-MK1 cells (Figure 16).

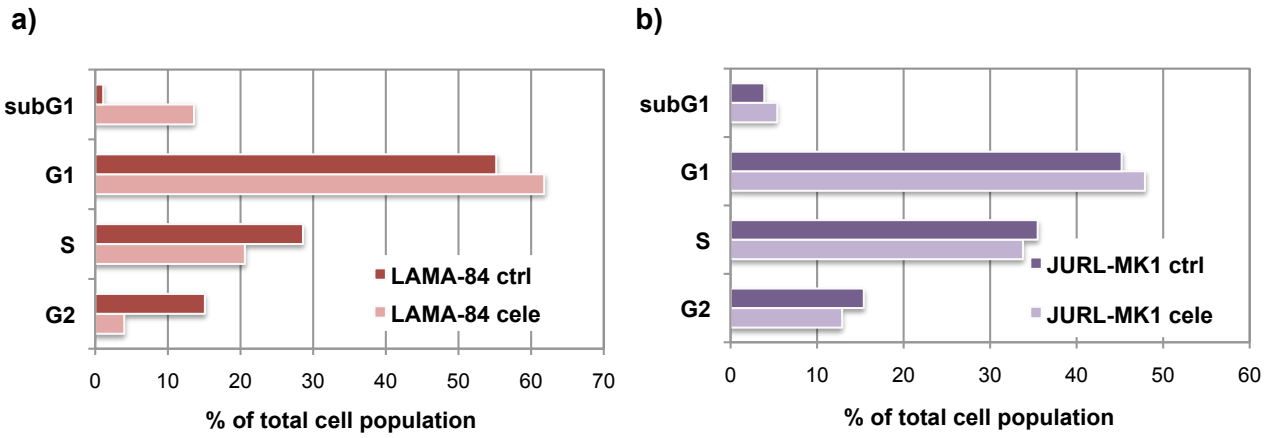

	SubG1	G1	S	G2
LAMA-84 ctrl	1,1	55,2	28,6	15,1
LAMA-84 celecoxib	13,6	61,8	20,6	4
JURL-MK1 ctrl	3,9	45,2	35,5	15,4
JURL-MK1 celecoxib	5,4	47,9	33,8	12,9

Figure 16. Cell-cycle distribution assessed by flow cytometry of LAMA-84 and JURL-MK1 cell lines.

LAMA-84 (**panel a**) and JURL-MK1 cells (**panel b**) were treated for 24 hours with 25 μM celecoxib (**cele**) and stained with propidium iodide. Histograms display percentages of cell populations in the different phases of the cell cycle. Values are the averages of three independent experiments (± standard error).

Data generated by flow cytometry were further supported by trypan blue exclusion tests (Figure 17) and microscopic counting of fragmented nuclei stained with the Hoechst-33258 florescent dye (Figure 18), which revealed that 25 μM celecoxib causes cell death only in the LAMA-84 cell line.

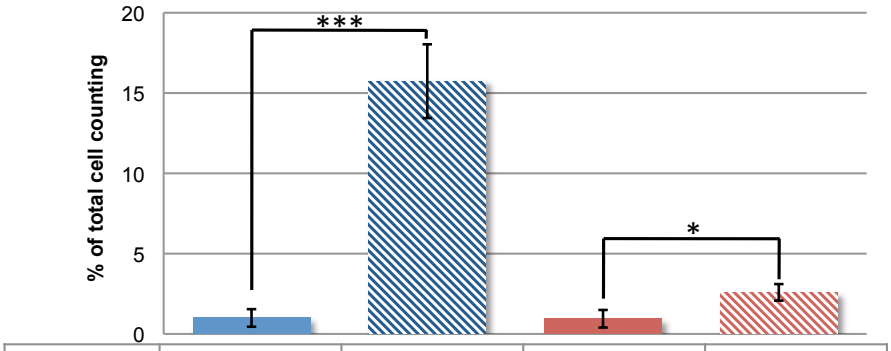

	LAMA-84 ctrl	LAMA-84 cele	JURL-MK1 ctrl	JURL-MK1 cele
Dead	1±0,547	15,74±2,298	0,95±0,549	2,59±0,516

Figure 17. Trypan-blue exclusion test on LAMA-84 and JURL-MK1 cell lines.

Cells were treated with 0.1% DMSO (**ctrl**) or 25 μM celecoxib (**cele**) for 24 hours. Histograms represent the percentages of, trypan blue-positive, dead cells. A minimum of 100 cells was scored in each condition. Values represent the means of three independent experiments (± standard error). **P ≤ 0,05, **P ≤ 0,01, ***P ≤ 0,001* (*student t-test*).

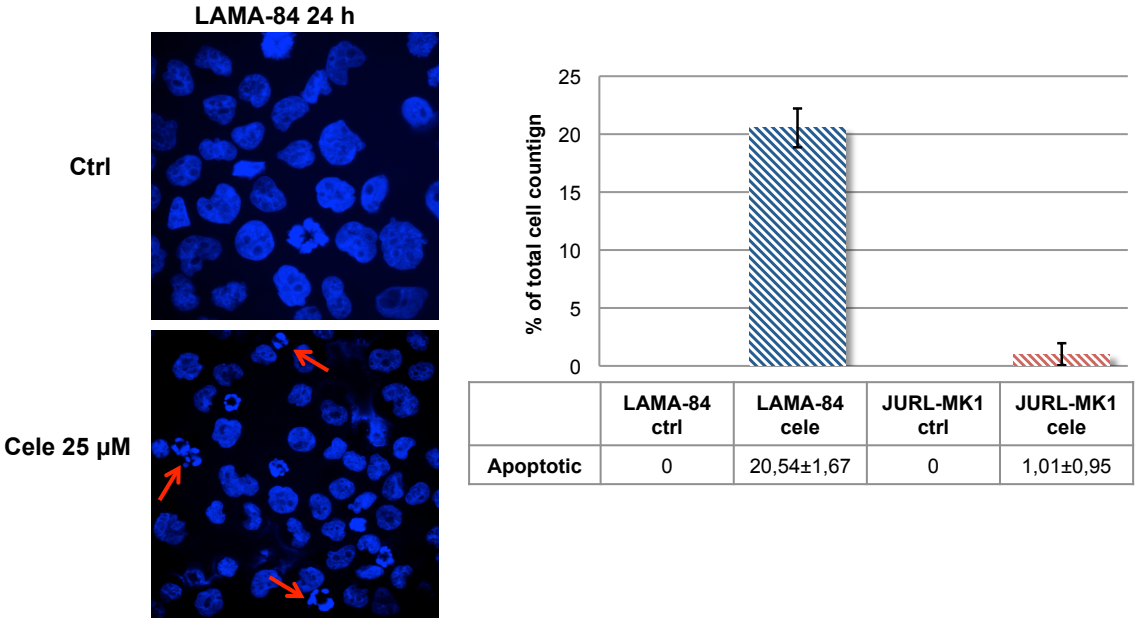

	LAMA-84 ctrl	LAMA-84 cele	JURL-MK1 ctrl	JURL-MK1 cele
Apoptotic	0	20,54±1,67	0	1,01±0,95

Figure 18. UV-fluorescent microscopy (600 X) of Hoechst33258-stained LAMA-84 and JURL-MK1 cell nuclei.

Cell lines were treated for 16 hours with 0.1% DMSO (**ctrl**) or 25 μM celecoxib (**cele**). Histograms represent the percentages of apoptotic cells presenting fragmented nuclei. Data express averages of three independent experiments (± standard error).

3.2 The effects of celecoxib are COX-2-independent

To investigate whether the anti-leukaemia effects of celecoxib are due to inhibition of one or both cyclooxygenase isoenzymes, COX-1 and COX-2, we analyzed the expression of these proteins in K562, LAMA-84 and JURL-MK1 cell lines. Immunoblots of protein lysates revealed that the three cell lines express only moderate levels of COX-1, whereas expression of the COX-2 isoenzyme was not detected (NIH-3T3 and MSTO-211H protein lysates were used as positive controls respectively for COX-1 and COX-2 proteins; Figure 19).

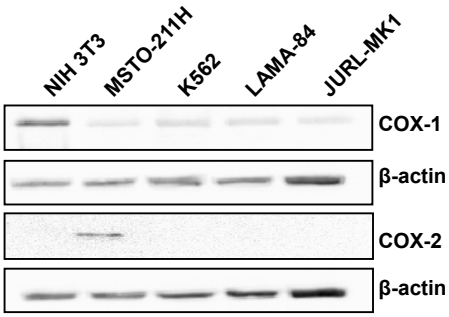

Figure 19. Protein levels of cyclooxygenase 1 (COX-1) and 2 (COX-2) in CML cell lines.

Immunoblots were performed combining a monoclonal anti-COX-1 primary antibody with an HRP-conjugated secondary antibody produced in mouse, or a polyclonal anti-COX-2 primary antibody with an HRP-conjugated secondary antibody produced in goat. β-actin levels were used to assess the equivalence of protein loadings.

To further confirm that the effects of celecoxib are COX2-independent, LAMA-84 and JURL-MK1 cell lines (for 24, 48 and 72 hours) were incubated with increasing concentrations of rofecoxib, another selective COX-2 inhibitor, and the 2,5-dimethyl derivative of celecoxib (DMC), which lacks COX-2-inhibitory function [55,56,62]. The effects of these drugs on the viability of CML cell lines was evaluated by the MTT assay. Treatment with DMC mimicked the anti-leukaemia effects of celecoxib, of which it is more potent (at least in the JURL-MK1 cells; Figure 20). By contrast, rofecoxib had no effect, regardless of the concentration used or the cell line in which it was tested (Figure 21).

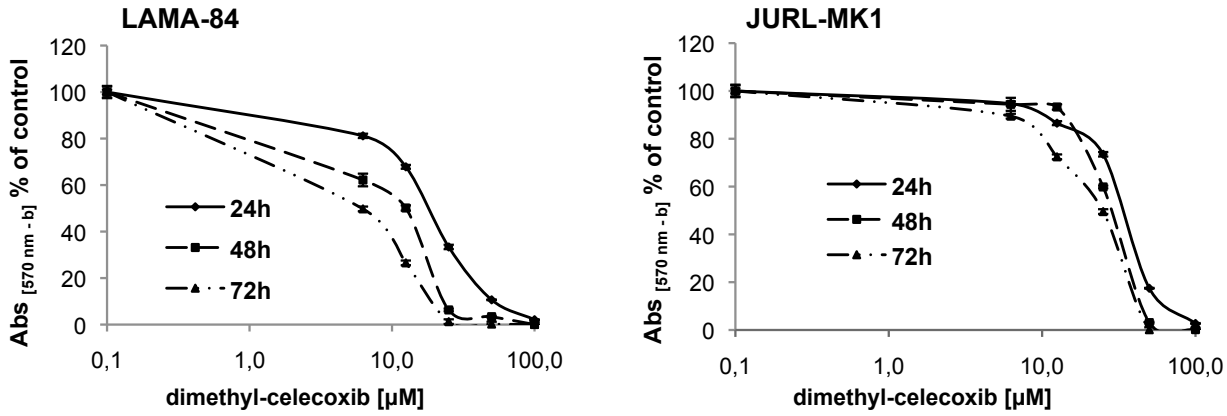

Figure 20. Cell viability evaluated by the MTT assay.

LAMA-84 and JURL-MK1 cell lines were treated with increasing concentrations (12.5, 25, 50, 100 µM) of dimethyl-celelcoxib for 24, 48 and 72 hours. Values represent the mean of three independent experiments (± standard error).

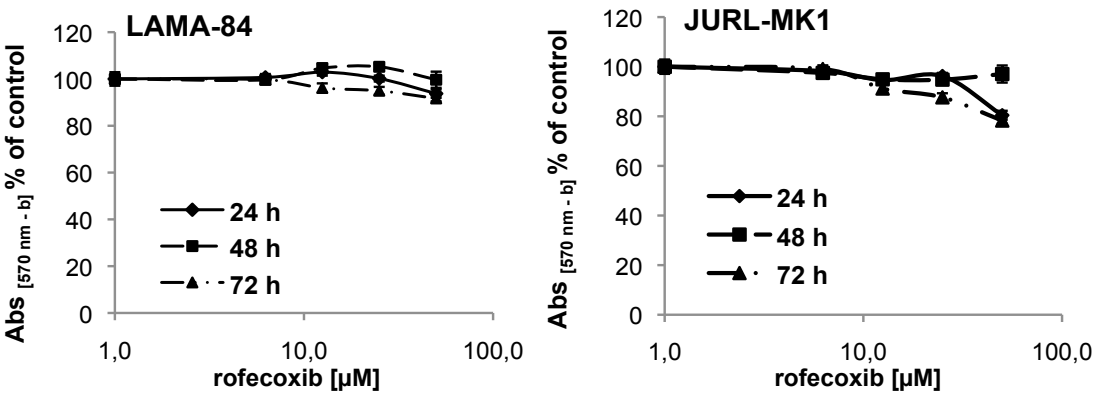

Figure 21. Cell viability, dose-response curves of LAMA-84 and JURL-MK1 evaluated by the MTT assay.

Cells were treated with increasing concentrations (6.25, 12.5, 25, 50 μM) of rofecoxib for 24, 48 and 72 hours. Data express the averages of three independent experiments (± standard error).

The therapeutic potential of putative anti-leukaemia drugs is also measured by their ability to suppress methylcellulose colony formation. Thus, LAMA-84 or JURL-MK1 cells were treated with increasing concentrations of celecoxib (or with vehicle, i.e. 0,1% DMSO), before plating equal numbers of cells (1,250 cells/well) into culture media containing 80% methylcellulose. Colonies were counted 6 days later and treatment with celecoxib suppressed colony formation in a concentration-dependent manner. While LAMA-84 cells were more sensitive than JURL-MK1 to treatment with celexoxib also in the clonogenic assays, the EC50 values for the methylcellulose assays (0,5 and 3,8 μM, respectively) (Figure 22) were markedly lower than for the MTT assays. In agreement to what was shown by the MTT assays, these effects did not rely on the inhibition of COX-2 since rofecoxib did not abolish or reduce, the formation of colonies in CML cell cultures, even at the 25 μM concentration (Figure 22).

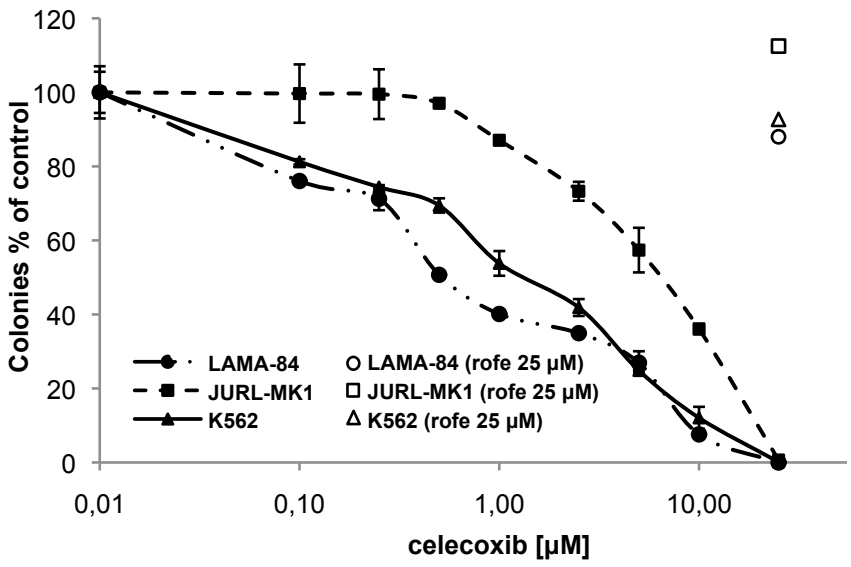

Figure 22. Clonogenic assay, dose-response curves of K562, LAMA-84 and JURL-MK1 cell lines (1250 cells/well) grown on 80% methylcellulose culture media.

CML cell lines were treated with celecoxib (0.1, 0.25, 0.5, 1, 2.5, 5, 10, 25 μM) or rofecoxib (**rofe**; 25 μM) for 6 days. Results are expressed as percentages of colonies counted in drug-treated groups as compared to 0.1% DMSO-treated controls. Values represent the mean of three independent experiments made in duplicate (± standard error).

3.3 The β-Catenin/Tcf/Lef axis is impaired by celecoxib

A great deal of attention has recently been paid to the role of signal transduction pathways that maintains the self-renewal of leukemic blasts. Like other types of leukaemias, CML stem-cells appear to rely on these pathways and in particular on the activation of the β-catenin/Tcf-Lef-dependent transcription program activated in normal cells by Wnt [(63)]. Indeed, it is becoming clear that this pathway is aberrantly activated in CML blasts both in the chronic phase and the blast crisis stage of the disease [(24)]. More intriguingly, recent studies have shown that BCR-ABL may sustain the activation of β-catenin independently of Wnt; in particular BCR-ABL can inhibit the glycogen synthase kinase 3β (GSK-3β) that regulates ubiquitination and proteasomal degradation of β-catenin, and activate the transcriptional function of β-catenin by direct phosphorylation on tyrosine residues [(17,45)].
Thus, we assessed the effects of celecoxib on β-catenin protein levels in drug-treated (25 μM; 2-24 hours) LAMA-84 and JURL-MK1 cells. Immunoblots of protein lysates probed with an antibody specific for β-catenin revealed that, in LAMA-84 cells, celecoxib treatment caused a marked decrease of β-catenin levels that was already visible after 2 hours, and reached a peak after 8-16 hours. By contrast, in JURL-MK1 cells, celecoxib had no effect on β-catenin protein levels at any time-point (Figure 23).

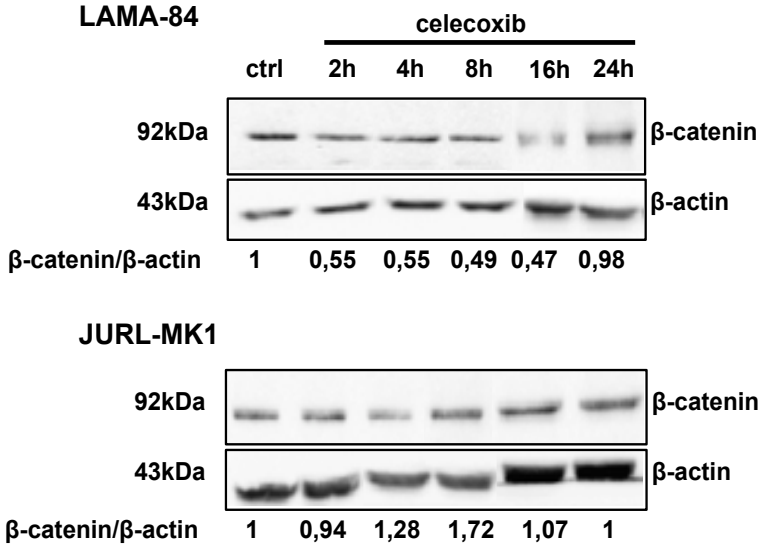

Figure 23. Protein levels of β-catenin in LAMA-84 and JURL-MK1 cell lines exposed to 25 μM celecoxib.

Cells were treated for 2, 4, 8, 16 and 24 hours before isolating protein lysates. Immunoblots were performed using a monoclonal anti-β-catenin primary antibody and a HRP-conjugated secondary antibody produced in mouse. Odds represent the "relative intensity" of β-catenin immuno-reactive bands corrected by the levels of β-actin, used to normalize protein loadings

Since the down-regulation of a given protein may be due to decreased expression or enhanced degradation, we assessed first, the effect of 25 μM celecoxib on β-catenin mRNA levels using the real-time PCR approach. As shown in Figure 24, already after 2 hours of treatment, celecoxib strongly reduced (almost by 80%) the expression of β-catenin mRNA in LAMA-84 cells. This effect, which lasted at least for 24 hours after a single administration of celecoxib, was not observed in the drug-resistant JURL-MK1 cell model (Figure 24).

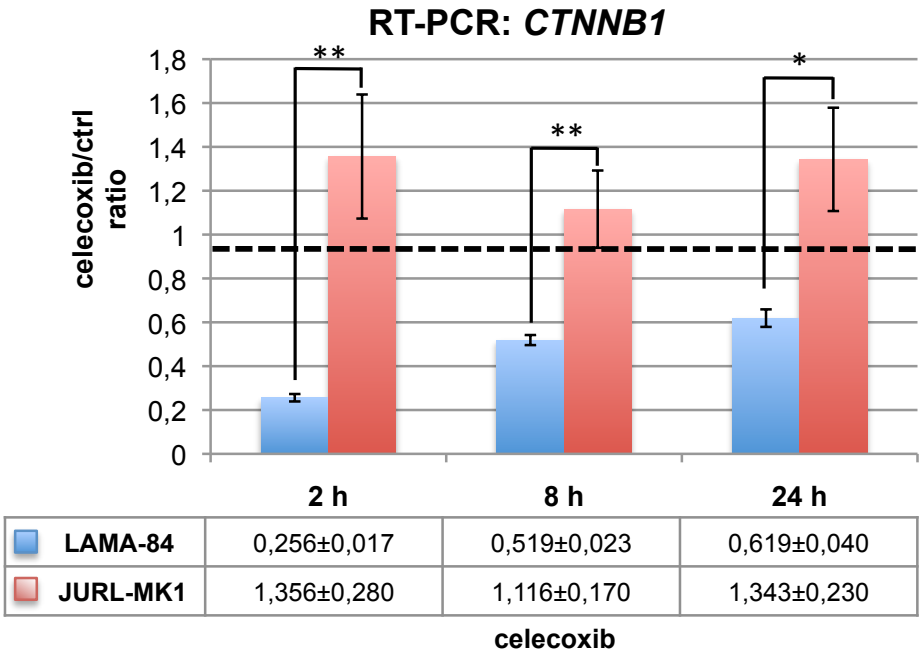

Figure 24. Transcriptional levels of the β-catenin gene (*CTNNB1*) in LAMA-84 and in JURL-MK1 cell lines treated for 2, 8 and 24 hours with celecoxib (25 μM).

Histograms represent the ratio between *CTNNB1* mRNA levels in celecoxib-treated or 0.1% DMSO-treated (**ctrl**) groups, which were measured by means of the real-time PCR technique. The levels of *CTNNB1* mRNAs were normalized using the expression of GAPDH as housekeeping gene. Values represent means of three independent experiments (± standard error). **P ≤ 0,05, **P ≤ 0,01, ***P ≤ 0,001* (*student t-test*).

On the other hand, since β-catenin protein stability is largely dependent on proteasomal degradation, we evaluated if the pharmacological inhibition of this process rescued the expression of the protein in the presence of 25 μM celecoxib. Indeed, levels of β-catenin protein detected in LAMA-84 cells treated with the proteasome inhibitor MG132 (20 μM), given alone, or in combination with 25 μM celecoxib (**Comb.**) were higher not only of those in cells treated only with celecoxib, but also of those of the 0.1 % DMSO-treated controls (Figure 25).

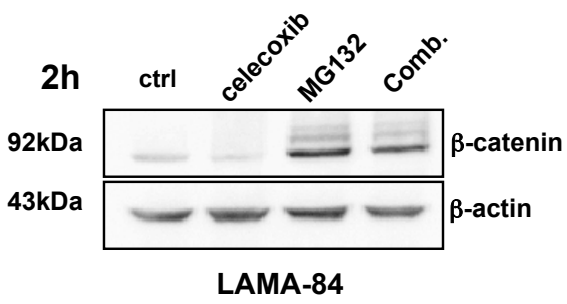

Figure 25. MG132 (a proteasome-specific inhibitor) reverts the effects of celecoxib on β-catenin protein degradation.

LAMA-84 cells were treated for 2 hours with celecoxib (25 μM) or MG132 (20 μM), alone or in combination (**Comb.**). Immunoblots were performed using a monoclonal anti-β-catenin primary antibody as described in Figure 23. The levels of β-actin are displayed as proof of equivalent loadings.

Since a precondition to proteasomal degradation of β-catenin is its GSK-3β-dependent phosphorylation on amino-terminal serine residues, we monitored the activity of this kinase following to treatment with 25 μM celecoxib. Thus, we measured the levels of the inactive form of GSK-3β generated via Akt-dependent phosphorylation of its serine-9 (ser-9) residue [(64)].

As shown in Figure 26, by comparing immunoblots of phospho-ser9 and total GSK3-β protein levels, it was evident that celecoxib, already after a 4-hours treatment, was able to inhibit ser-9 phosphorylation, restoring the activity of this kinase. By contrast, celecoxib did not affect the phosphorylation of GSK-3β in the more resistant JURL-MK1 cells (Figure 26).

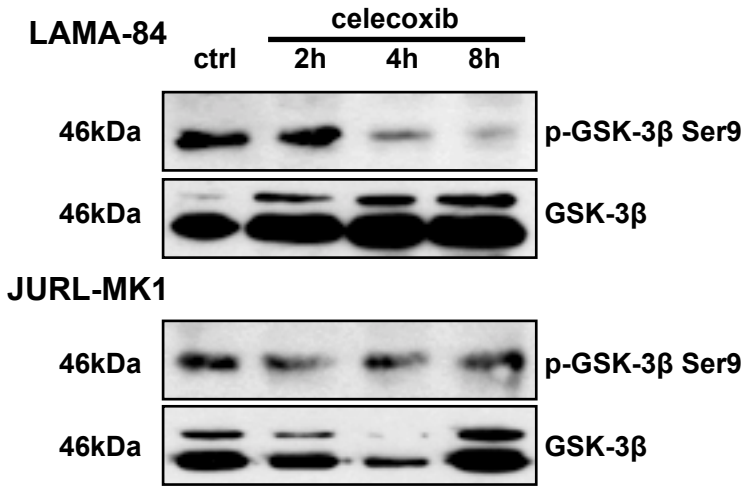

Figure 26. Celecoxib restores GSK-3β activity.

After 2, 4 and 8 hours in presence of 25 μM celecoxib, LAMA-84 and JURL-MK1 protein lysates were probed with a primary antibody specific for the phospho-serine 9 epitope of GSK-3β (**p-GSK-3β Ser9**) and detected by using a HRP-conjugated secondary antibody produced in rabbit. Levels of total GSK-3β protein were assessed to equalize protein loadings.

The role of GSK3-β re-activation in the celecoxib-induced degradation of β-catenin was clearly demonstrated by using this drug in presence of an inhibitor of this kinase. Indeed, LAMA-84 cells treated for 4 hours with the GSK3-β inhibitor, BIO (10 μM), given alone or in combination with 25 μM celecoxib (**Comb.**) displayed levels of β-catenin higher than those detected in celecoxib- or in 0.1 % DMSO-treated controls (Figure 27).

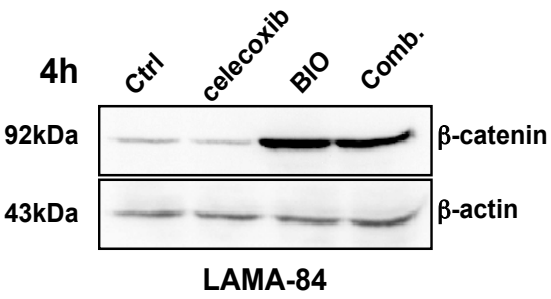

Figure 27. Celecoxib restores GSK-3β activity.

LAMA-84 cells were treated for 4 hours alternatively with: 25 μM celecoxib, 10 μM BIO, or a combination of both (**Comb.**). Protein lysate were probed with an anti-β-catenin mouse monoclonal antibody and HRP-conjugated secondary antibodies produced in mouse. β-actin levels are displayed as proof of equal loadings.

Previous studies showed that cytosolic stabilization of unphopshorylated β-catenin allows the translocation into the nucleus to form complexes with transcriptional factors of the Tcf (T-cell factor)/Lef (lymphoid enhancing factor) family [23,28]. Thus, by immnublotting protein lysates of LAMA-84 cells with an antibody recognizing only the unphosphorylated form of β-catenin (actβ-cat), we observed that celecoxib was able to reduce the levels of the transcription-competent form of this protein in a time- (Figure 28a) and concentration-dependent manner (Figure 28b). These effects were also evident after correcting the levels of active β-catenin by the total levels of this protein (Figure 28b). On the other hand, celecoxib was not able to affect the levels of active- β-catenin when testing the drug-resistant cell line JURL-MK1 (Figure 28a).

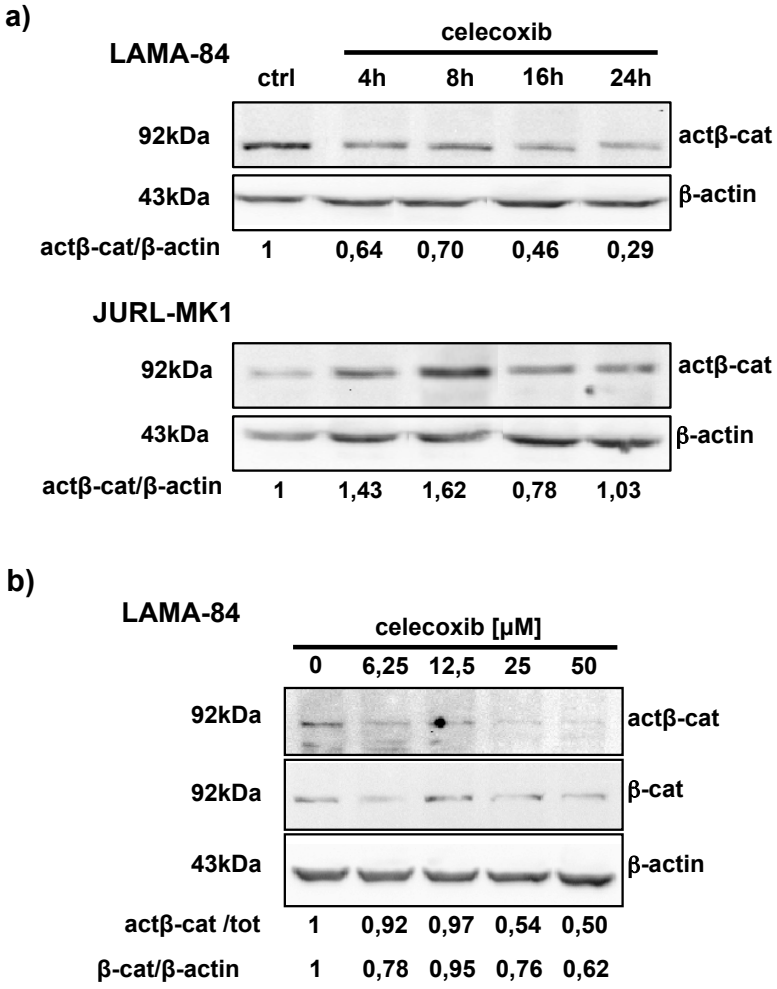

Figure 28. Celecoxib reduces the levels of the transcriptional-active form of β-catenin (act-β-cat) in a time and concentration dependent manner.

a) LAMA-84 and JURL-MK1 cell lines were treated for 4, 8, 16 and 24 hours with 25 μM celecoxib. Immunoblots on protein lysates were performed using a polyclonal antibody that recognize β-catenin only when unphosphorylated at the Ser33/37/Thr41 epitopes (the transcriptional-active form; **act-β-cat**). A HRP-conjugated secondary antibody produced in rabbit was used for detection. Odds represent the "relative intensity" of act-β-cat immuno-reactive bands corrected by the levels of β-catenin whole protein. The levels of β-actin were used to normalize protein loadings between lanes. **b)** LAMA-84 cells were treated for 24 hours with increasing concentration of celecoxib (6.25, 12.5, 25, 50 μM) before probing protein lysates with the antibody that recognizes the act-β-cat isoform. A HRP-conjugated secondary antibody produced in mouse was used for detection. Ratios of act-β-cat/β-cat "relative intensity" are displayed as in **(f)**. β-actin levels were used to normalize protein loadings between lanes.

As stated above, the β-catenin/Tcf/Lef complex transactivates genes involved in cell growth or with anti-apoptotic functions. One of such target genes is the *c-myc* oncogene; thus, to further demonstrate that celecoxib inhibits the transcription-regulatory activity of β-catenin, we performed quantitative real time PCR analysis of *c-myc mRNA* levels. Indeed, exposure of LAMA-84 cells to 25 μM celecoxib (for 2, 8 or 24 hours) caused a dramatic decrease (more evident after 8 hours) in the levels of *c-myc* transcripts (Figure 29), an effect that was confirmed also by assessing the levels of the protein (data not shown).
It is also known that nuclear accumulation of β-catenin impairs the transcription of the *CDKN2A* gene, which encodes the $p16^{INK4a}$ tumor suppressor protein, with an inhibitory effect on cell cycle progression [23,65]. Real Time PCR of *CDKN2A* mRNA levels assessed after treatment with 25 μM celecoxib (time-course of 2, 8, and 24 hours) revealed a significant increase of *CDKN2A* mRNA transcripts, although only after a 24-hours treatment (Figure 29).

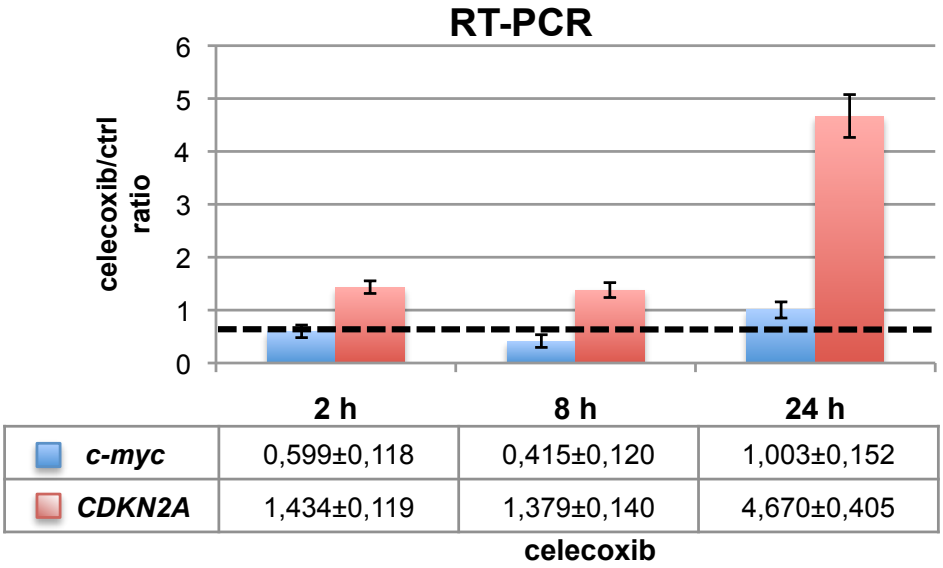

Figure 29. Celecoxib affects the transcription of β-catenin-target genes *c-myc* and *CDKN2*.

LAMA-84 cells were treated for 2, 8 and 24 hours with 25 μM celecoxib. For each of the genes tested, histograms represent the ratio between mRNA levels in celecoxib-treated or 0.1% DMSO-treated (**ctrl**) groups, which were measured by means of the real-time PCR technique. Data were normalized using the expression of GAPDH as housekeeping gene. Values represent means of three independent experiments (± standard error).

To establish a correlation between the biochemical and biological effects of celecoxib, we generated a LAMA-84 parental cell line expressing a constitutively active mutant form of β-catenin in which serine 33 is replaced by a tyrosine residue (β-catenin S33Y) that is not recognized by GSK-3β, thus preventing the proteolytic degradation of β-catenin [27,28].
Then, following to treatments with celecoxib, we assessed viability and proliferation of the β-catenin-S33Y cell line, through concentration-response experiments using MTT and clonogenic assays, in comparison to parental LAMA-84 cells. As expected, cells expressing the degradation-resistant form of β-catenin (β-catenin-S33Y) were significantly more resistant than wild-type cells, to either acute (Figure 30a, upper panel) or chronic (Figure 30b, lower panel) exposure to celecoxib.

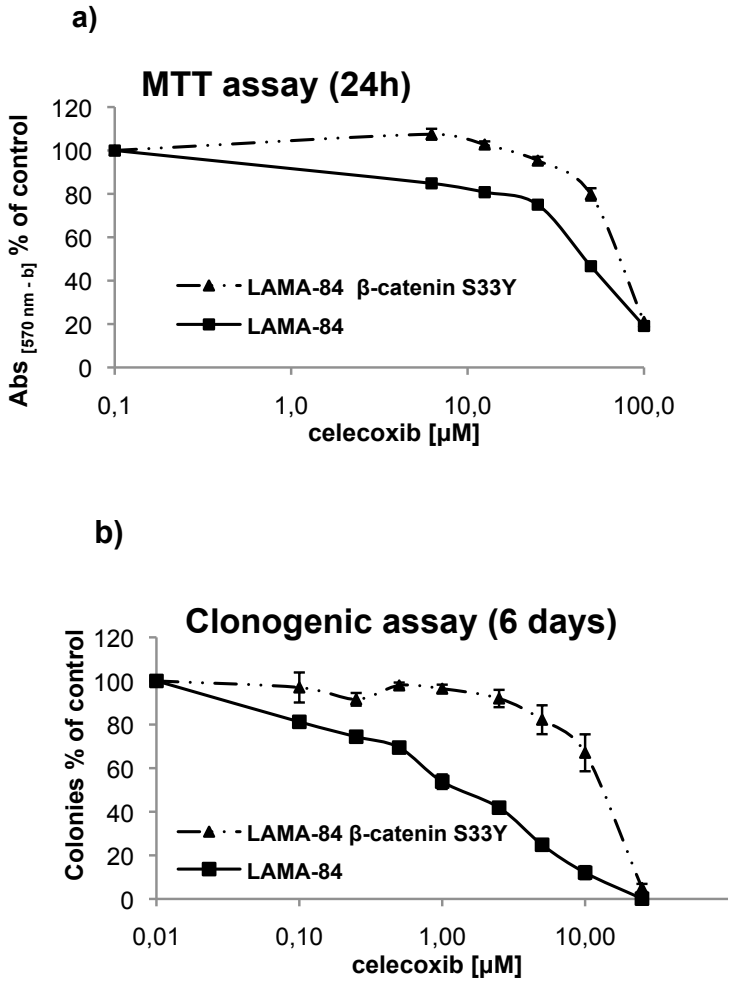

Figure 30. Cell viability of LAMA-84 cells expressing wild-type (LAMA-84) or an "undegradable" mutant (LAMA-84 β-catenin S33Y) of β-catenin.

Upper panel (**a**) displays the result of the MTT assay after 24 hours treatments with increasing concentrations of celecoxib (6.25, 12.5, 25, 50, 100 μM). Lower panel (**b**) displays the result of the clonogenic assay after 6 days in presence of increasing concentrations of celecoxib (0.1, 0.25, 0.5, 1, 2.5, 5, 10, 25 μM). Results are expressed as percentages of colonies counted in drug-treated groups as compared to 0.1% DMSO-treated controls. Data express averages of three independent experiments made in duplicate (± standard error).

3.4 Celecoxib inhibits the mammalian target of rapamycin-complex 1 (mTORC1) while sparing complex 2 (mTORC2)

Given the ability of celecoxib to re-activate GSK-3β, we tested the hypothesis that the anti-leukaemic effects of this drug may depend, in part, on the inhibition of the mammalian target of rapamycin (mTOR). Indeed, it is known that GSK-3β exerts an inhibitory effect on mTORC1 by phosphorylating the tuberous sclerosis 2 protein (TSC2), which is endowed with a GTPase-activating function [32,33]. In turn, such phosphorylation of TSC2 causes its activation and the consequent inhibition of Rheb, the small G-protein indispensable for mTORC1 activity. An effect on this pathway may explain, in part, the effects of celecoxib in CML cells since mTOR plays a critical role in the growth and survival of BCR-ABL transformed cells [20,31,34].

To determine whether celecoxib inhibits mTOR activation, we evaluated the effect of the drug on the phosphorylation of this protein and its downstream targets.

Immunoblots of LAMA-84 and JURL-MK1 protein extracts with anti-phospho-mTOR specific antibodies allowed discrimination, upon treatment with celecoxib (25 μM, given for 2, 4, 16 and 24 hours), between phosphorylation of serine 2448 and of serine 2481, characteristic of, respectively, mTORC1 and mTORC2 activation. As shown in Figure 31, only in the LAMA-84 cell line, celecoxib was able to induce a significant decrease of serine 2448 phosphorylation, an effect that was maximal within 4 hours of treatment. Importantly, phosphorylation of mTOR on serine 2481 was not affected by the treatment, suggesting that inhibition of mTORC1 did not cause the compensatory activation of mTORC2, usually observed after treatments with rapamycin and congeners.

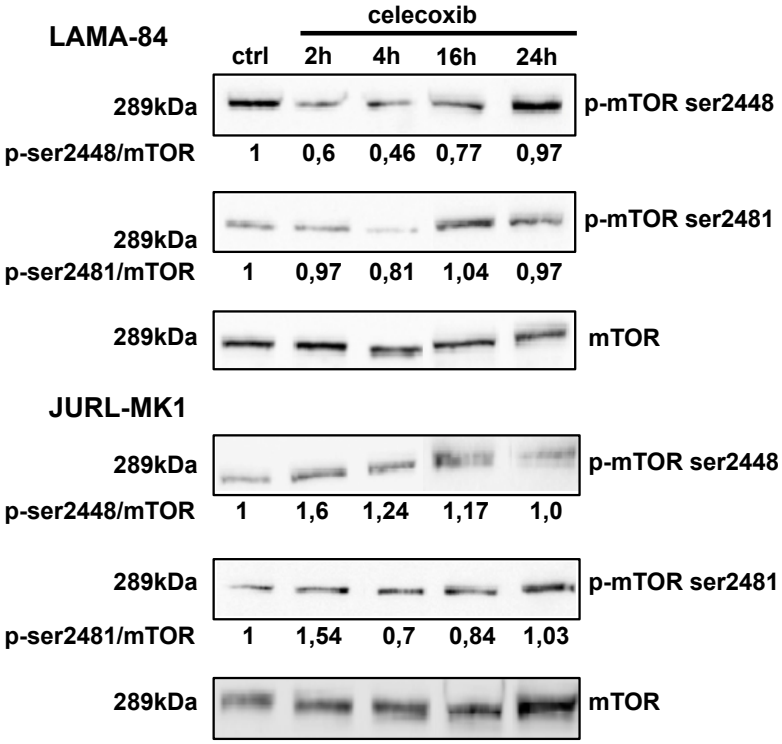

Figure 31. Characterization of mTORC1 vs mTORC2 signalling in LAMA-84 and JURL-MK1 cell lines treated for 2, 4, 16 and 24 hours with celecoxib (25 μM).

Protein lysates were blotted using primary polyclonal antibodies specific for: mTOR whole protein; mTORC1, identified by the phospho-serine 2448 epitope (**p-mTOR ser2448**), mTORC2, presenting the phospho-serine 2481 epitope (**p-mTOR ser2481**). HRP-conjugated secondary antibodies, produced in rabbit, were used for detection. Odds represent the "relative intensity" of phospho-mTOR immuno-reactive bands corrected by the levels of the whole kinase.

In agreement with the finding of mTORC1 inhibition, celecoxib was able to reduce the phosphorylation of the two most important targets of mTORC1, i.e. the S6 Kinase (p70-S6K) and eIF4E binding protein (4E-BP1). Indeed, as shown in Figure 32, in the highly sensitive LAMA-84 cells, celecoxib suppressed the phosphorylation of p70S6K on threonine 389, significantly reducing also the accumulation of hyper-phosphorylated forms of 4E-BP1.

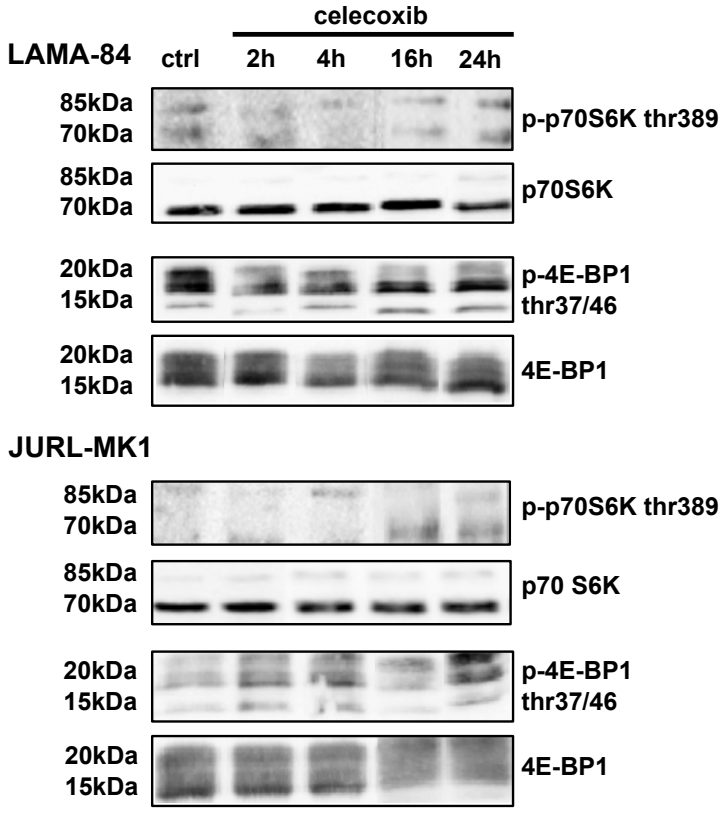

Figure 32. Activation of the mTORC1 down-stream targets in LAMA-84 and JURL-MK1 cell lines exposed to 25 μM celecoxib for 2, 4, 16 and 24 hours.

Protein lysates were probed with primary polyclonal antibodies specific for: the p70S6 kinase (**p70S6K**) or its active form, phosphorylated on threonine 389 (**p-p70S6K thr389**); 4E-BP1 or its active form, phosphorylated on threonine 37 and 46 (**p-4E-BP1 thr37/46**). HRP-conjugated secondary antibodies, produced in rabbit, were used for detection. Levels of p70S6K and 4E-BP1 are displayed as proof of equal loadings.

To confirm the ability of celecoxib to impair mTORC1 function, we measured the biological impact of a combined treatment (**Comb.**) with PP242, a catalytic inhibitor of mTOR. In order to do this, we analyzed the viability of LAMA-84 cells by MTT and clonogenic assays using concentrations of the two drugs close to their EC25 calculated in each test. Following to 24 hours of treatments, the MTT assay revealed that the effects of 12,5 μM celecoxib and 50 nM PP242 were additive (Figure 33a). Conversely, clonogenic assays performed in the presence of much lower concentrations of the two drugs (250 nM

celecoxib; 5 nM PP242) minimally increased the effect induced by each compound alone (Figure 33b), thus suggesting a redundant mechanism of action.

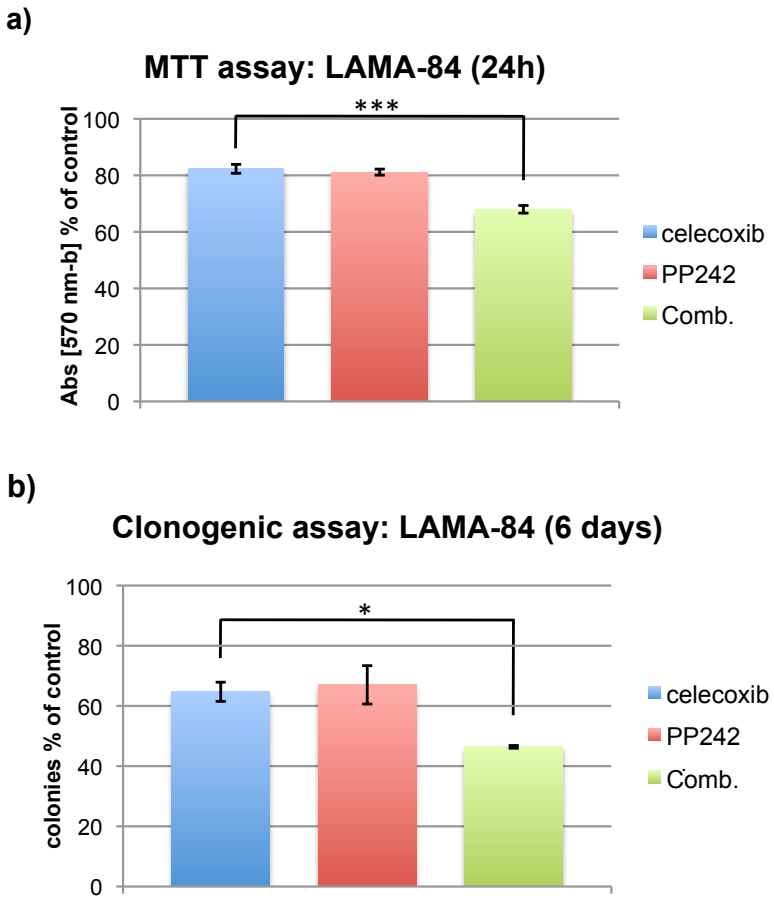

Figure 33. Antiproliferative effects of celecoxib given in combination with a mTOR catalytic inhibitor.

a) Viability of LAMA-84 cells treated for 24 hours with 12,5 μM celecoxib, 50 nM PP242, or a combination (**Comb.**) of both, was determined by using the MTT assay. Values represent the mean of three independent experiments (celecoxib 82,30±7,718; PP242 81,14±5,448; Comb. 67,98±6,907). **P ≤ 0,05, **P ≤ 0,01, ***P ≤ 0,001* (*student t-test*). **b)** Clonogenic assay, dose-response curve of LAMA-84 cells grown for 6 days on 80% methylcellulose (1250 cells/well) after exposure to 250 nM celecoxib, 5 nM PP242, or a combination (**Comb.**) of both. Results are expressed as percentages of colonies counted in drug-treated groups as compared to 0.1% DMSO-treated controls. Data represent the averages of three independent experiments made in duplicate (celecoxib 64,7±3,188; PP242 67,0±6,376; Comb. 46,4±0,455). **P ≤ 0,05, **P ≤ 0,01, ***P ≤ 0,001* (*student t-test*).

3.5 The activation of the AMP-activated protein kinase (AMPK) is involved in the effect of celecoxib

It was previously shown that, in order to fully activate TSC2, GSK-3β requires an AMPK-dependent phosphorylation of this GAP [34], thus supporting a synergistic function of the two kinases that are under the control of metabolic and growth factor signals [31,66]. With this in mind, we assessed whether celecoxib treatment influences the serine/threonine kinase function of AMPK in order to allow a complete inhibition of mTOR via TSC2 phosphorylation.
Using an antibody that specifically recognizes phosphorylated threonine 172 of the alpha subunit of AMPK, which identify the catalytic active form of the kinase, we performed immunoblots on protein extracts of CML cell lines exposed to celecoxib (25 μM). As shown in Figure 34, only in the LAMA-84 cell line celecoxib was able to increase AMPK phosphorylation as soon as 15 minutes after treatment, with a maximal effect after 30 minutes.

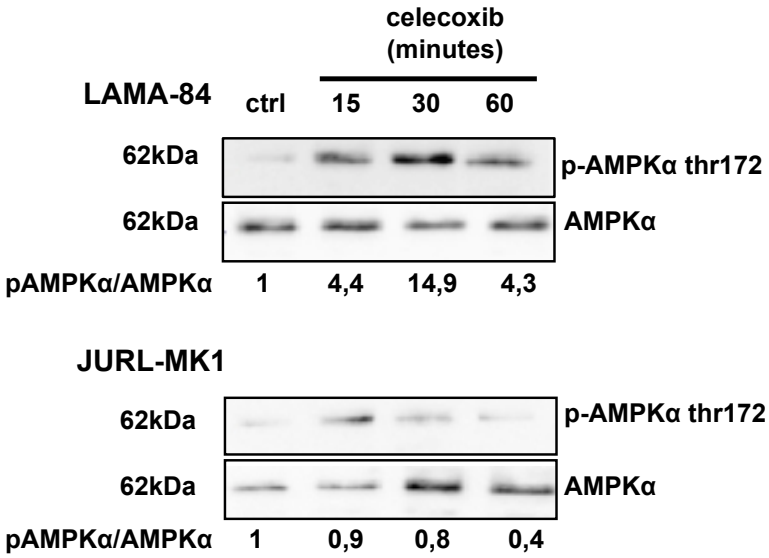

Figure 34. Activation of AMPK in LAMA-84 cells treated with 25 μM celecoxib.

LAMA-84 and JURL-MK1 cell lines were treated for 15, 30 minutes, 1 and 2 hours with celecoxib before probing protein lysates with polyclonal antibodies that recognize: the AMPKα subunit or its active form, phosphorylated on threonine 172 (**p-AMPKα thr172**). HRP-conjugated secondary antibodies, produced in rabbit, were used for detection. Odds represent the "relative intensity" of phospho-AMPKα immuno-reactive bands corrected by the levels of the whole protein.

Since AMPK can be activated either in response to a reduction in cell energy, represented by a relative increase of AMP over ATP concentrations, an event mediated by the tumor suppressor LKB1, or by the activation of the Ca^{2+}/calmodulin-dependent kinase kinase β (CaMKKβ)[31,39], we investigate which of the two pathways mediates the effect of celecoxib

on AMPK activation. In order to do this, we used 25 μM celecoxib to treat the LKB1-deficient human cell line HeLa (presenting a strong methylation in the promoter of this gene)[39], before probing protein with antibody directed against the active form of AMPK. As displayed in Figure 35, also HeLa cells responded with a phosphorylation of AMPK on threonine 172 when challenged with celecoxib, suggesting that LKB1 is dispensable for this activity of the drug. Indeed, co-administration of the CaMKKβ specific inhibitor, STO-609 (2.5ug/mL, given as a 4 hours pre-treatment) completely abolished the phosphorylation of AMPK (Figure 35). Next, the ability of STO609 to abolish celecoxib-induced activation of AMPK was confirmed by immunoblots on LAMA-84 protein extracts (Figure 36).

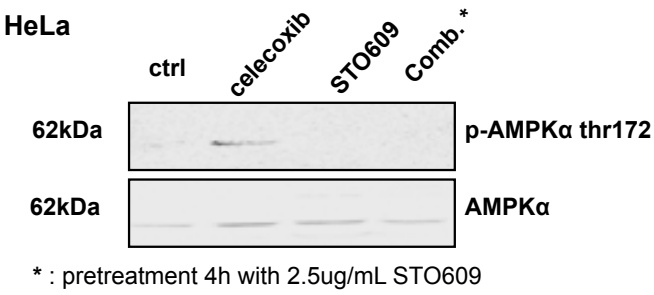

Figure 35. Celecoxib-induced activation of AMPK relies on Ca^{2+}/Calmodulin kinase kinase β (CaMKKβ) function.

HeLa cells, which are intrinsically devoid of the AMPK primary up-stream activator liver kinase B1 (LKB1), were treated with 25 μM celecoxib (for 30 minutes), the CaMKKβ inhibitor STO609 (2,5 mg/mL, 4 hours), or a combination of both (**Comb.**; STO609 was given as a 4 hours pre-treatment). Protein lysates were probed with anti-phospho-AMPKα antibody as described in Figure 34.

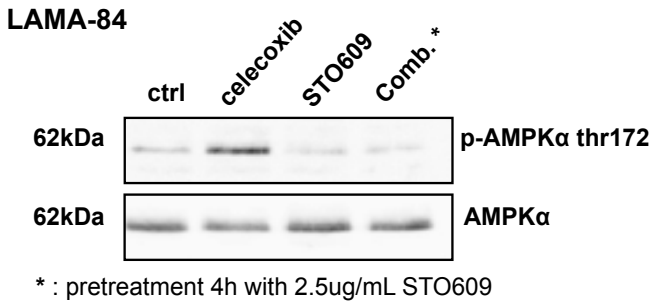

Figure 36. CaMKKβ inhibition impairs the effect of celecoxib also in the LAMA-84 CML cell line.

Immunoblots of LAMA-84 protein lysates probed with anti-AMPK antibodies (as in Figure 34 after treatments with 25 μM celecoxib (30 minutes), STO609 (2,5 mg/mL, 4 hours) or a combination of both (**Comb.**; STO609 was given as a 4 hours pre-treatment).

Moreover, to assess whether CAMKKβ-induced activation of AMPK plays a role in the anti-proliferative function of celecoxib, LAMA-84 cells were simultaneously treated with 25 μM celecoxib and STO-609. Although the CAMKKβ inhibitor displayed an intrinsic toxicity (a 20% decrease in the absorbance of the MTT assay as compared to untreated controls), this drug still significantly reduced the effect of celecoxib when used combination with it (42,2% vs 53,8% absorbance compared to untreated controls; Figure 37).

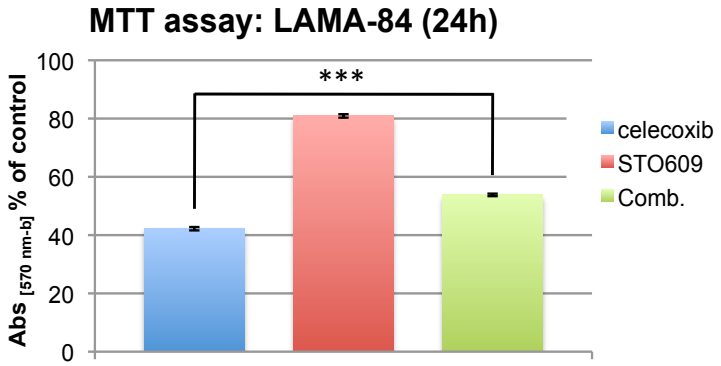

Figure 37. Cell viability of LAMA-84 cells treated for 24 hours with 25 μM celecoxib, 2,5 mg/mL STO609.

Histograms represent percentages of reduction of MTT values in drug-treated samples as compared to 0.1% DMSO-treated groups. Values are the mean of three independent experiments (celecoxib 42,2±0,578; STO609 80,9±0,595; Comb 53,8±0,436). **P ≤ 0,05, **P ≤ 0,01, ***P ≤ 0,001* (*student t-test*).

To provide final demonstration of the role played by AMPK in the anti-leukaemic effect of celecoxib, we knocked-down the expression of this kinase using a lentivirally delivered microRNA (AMPKα⁻) that targets the α1 catalytic subunit of the protein. By this approach we obtained only about a 54% reduction in the expression of AMPK, compared to the levels of this protein in cells treated with a non-targeting sequence (SCR; inset in Figure 38). Nevertheless, clonogenic assays on LAMA-84 SCR and AMPKα-silenced cells showed a clear shift to the right in the concentration-response of the cell line expressing lower levels of the kinase (Figure 38).

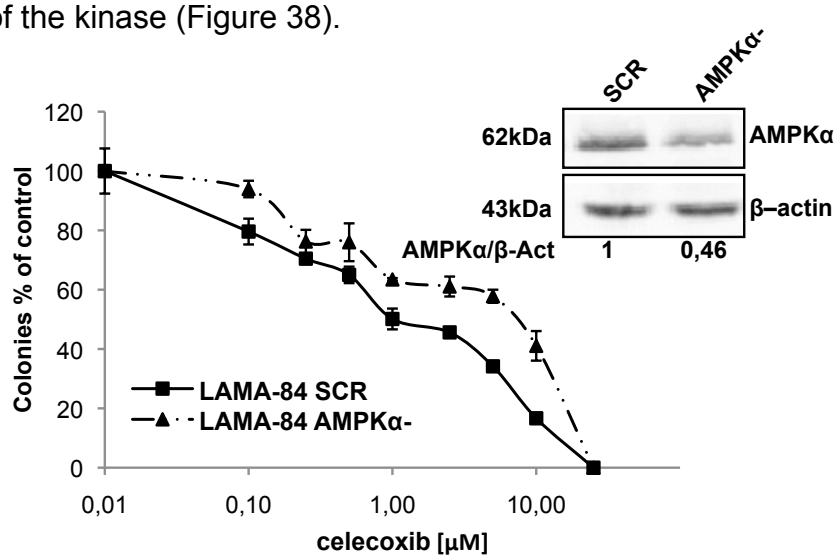

Figure 38. Clonogenic assay, dose-response curves of AMPK "knocked-down" (AMPKα⁻) vs "scramble-treated" (SCR) LAMA-84 cells exposed to increasing concentrations of celecoxib (0.1, 0.25, 0.5, 1, 2.5, 5, 10, 25 μM) and grown into 80% methylcellulose.

Cells were seeded at 1250 cells/well density and colonies were scored after 6 days. Results are expressed as percentage of the colonies counted in the 0.1% DMSO-treated group (control). Data are the averages of three independent experiments made in duplicate, (± standard error). In the inset, are displayed protein levels of AMPKα in cells exposed to lentivirally delivered scrambled (SCR) or AMPKα-targeted (AMPKα⁻) miRNAs. Immunoblots were obtained combining a polyclonal anti-AMPKα primary antibody with the HRP-conjugated secondary antibody produced in rabbit. Odds represent the "relative intensity" of AMPK immune-reactive bands corrected by the levels of β-actin used for loading normalization.

As proof-of-principle that AMPK is the most upstream effector of celecoxib-induced anti-leukaemic pathway, immunoblots on SCR and AMPKα-silenced LAMA-84 cell lysates demonstrated that a reduced expression of AMPK abrogates the effect of 25 μM celecoxib on the down-regulation of β-catenin (Figure 39).

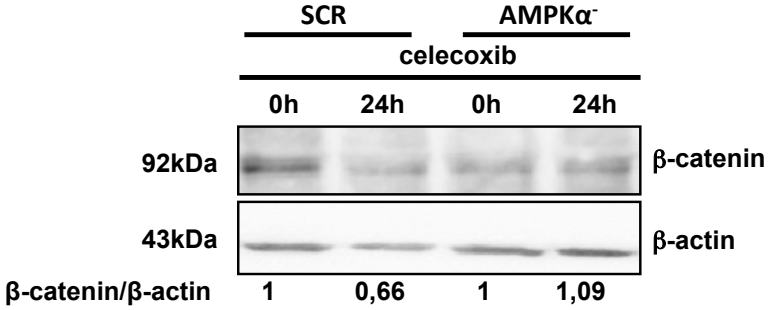

Figure 39. Expression of β-catenin protein in AMPKα- vs SCR LAMA 84 cells exposed to 25 μM of celecoxib for 24 hours.

Immunoblots of protein lysates were performed combining a monoclonal anti-β-catenin primary antibody and the HRP-conjugated secondary antibody produced in mouse. Odds represents the "relative intensity" of -β-catenin immune-reactive bands corrected by the levels of β-actin, used for loading normalization.

3.6 Potential impact of celecoxib on CML-targeting therapies

Previous studies demonstrated that treatment of CML cells with tyrosine-kinase inhibitors (TKI, e.g. imatinib), causes the activation of the autophagic response, and that process is detrimental for the therapeutic outcome [44]. Thus, we assessed the autophagic response in CML cell lines treated with active concentrations of celecoxib. .

Protein lysates of cell lines cultured for 24 h in presence of 25 μM celecoxib were blotted with an antibody recognizing both the cytosolic (LC3-I) and autophagosomal-associated (LC3-II) forms of the autophagy-specific marker microtubule-associated protein 1 light chain 3 (LC3). Moreover, since LC3-II accumulation may be consequent not only to the induction of autophaghy but also to the inhibition of autophagosome brake up [44,67], we tracked the so-called "autophagic flux" by adding 5 μM chloroquine (CQ) to treatments, in order to block lysome-dependent digestion of the vacuoles. As shown in Figure 40, the difference in the LC-I/II ratio in cells exposed to celecoxib or to vehicle (0.1 % DMSO) was negligible, while co-treatments with CQ revealed that celecoxib did not increase the levels of LC3-II generated by exposure to the lysomotropic agent alone. Of note, celecoxib-sensitive (LAMA-84) and celecoxib-resistant cells (JURL-MK1) gave similar results in this assay (Figure 40).

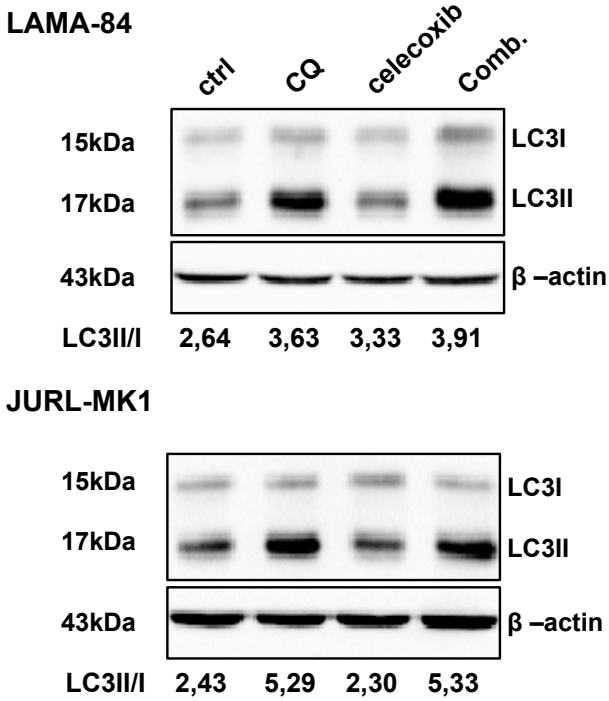

Figure 40. The effect of celecoxib on CML cell autophagy.

Evaluation of the "autophagic flux" of LAMA-84 and JURL-MK1 treated with 25 μM celecoxib, 5 μM chloroquine (**CQ**), or a combination of both (**Comb.**; CQ was given as 1 hour pre-treatment)**.** After 24 hours of incubation with drugs, protein lysates were probed with the anti-LC3B primary antibody in order to discriminate the unmodified protein (**LC3I**) from its phosphatydylethanolamine-conjugate (**LC3I**), used as marker of active autophagy (see the results). A HRP-conjugated secondary antibody, produced in rabbit, was used for detection. Odds (**LC3II/LC3I ratio**) represent the "relative intensity" of LC3II immune-reactive bands corrected by the levels of unmodified LC3B. Levels of β-actin are shown as proof of equal loadings.

On the other hand, visualization of autophagosomes by confocal microscopy of CML cell lines stained with a fluorescently-labelled anti-LC3 antibody demonstrated that celecoxib caused, at least in the LAMA-84 cell model, a modest increase in the percentage of cells displaying five or more LC3-positive vacuoles as compared to controls (0.1 % DMSO) and CQ-treated groups (Figure 41). Nevertheless, the effect of celecoxib was not potentiated by co-administration of CQ, suggesting that these drugs may share the inhibitory function on latest stages of autophagy.

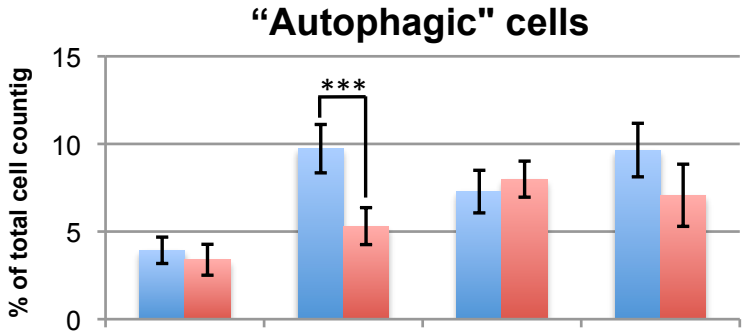

	ctrl	celecoxib	CQ	Comb.
LAMA-84	3,93±0,753	9,73±1,380	7,28±1,214	9,65±1,527
JURL-MK1	3,39±0,882	5,31±1,054	7,99±1,029	7,07±1,773

Figure 41. Scoring of "autophagic" cells by the presence of LC3B-positive cytosolic vesicles.

LAMA-84 or JURL-MK1 cells were treated for 24 hours as described for Figure 40**.** Histograms represent percentages of cells presenting at least 5 cytosolic vesicles positively stained by the anti-LC3 antibody. 0.1 % DMSO-treated cells were used as controls (**ctrl**). Values are the means of three independent experiments (± standard error). **P ≤ 0,05, **P ≤ 0,01, ***P ≤ 0,001* (*student t-test*).

Although of a limited entity, the biological impact of celecoxib-induced autophagy was evaluated through clonogenic assays. Co-treatment of LAMA-84 or JURL-MK1, with celecoxib and CQ, demonstrated that there was no further decrease in the number of colonies compared to that of cells treated with celecoxib alone (using sub-optimal concentrations of the drug, close to its EC25 calculated for each cell line) (Figure 42).

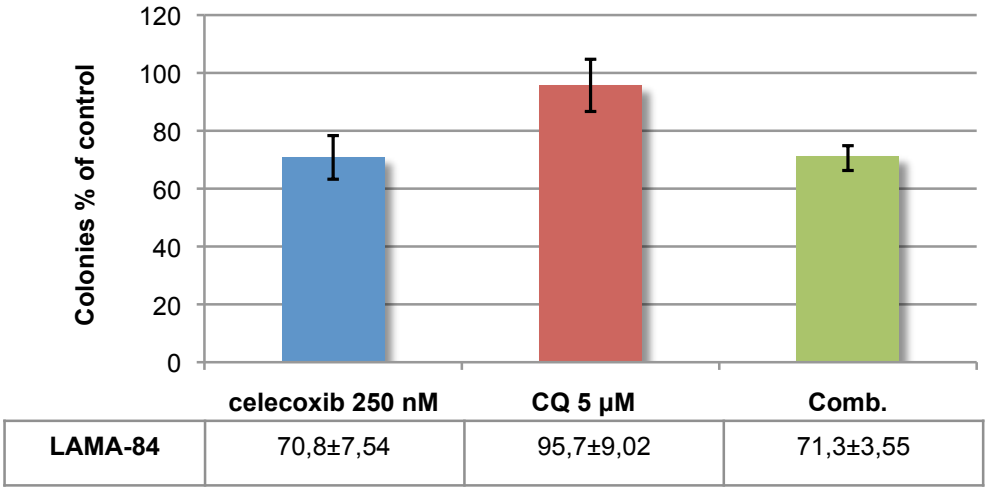

	celecoxib 250 nM	CQ 5 µM	Comb.
LAMA-84	70,8±7,54	95,7±9,02	71,3±3,55

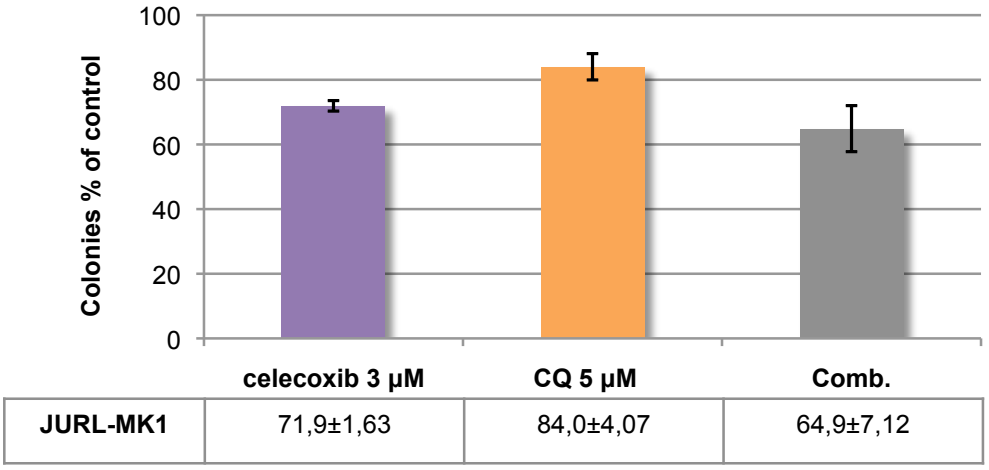

	celecoxib 3 µM	CQ 5 µM	Comb.
JURL-MK1	71,9±1,63	84,0±4,07	64,9±7,12

Figure 42. Clonogenic assay, of LAMA-84 and JURL-MK1 cell lines cultured for 6 days on 80% methylcellulose after exposure to celecoxib, CQ (5µM), or a combination of both (Comb.).

Celecoxib was administered for 6 days at concentrations near the EC25, as previously calculated through clonogenic assays (250 nM for LAMA-84; 3 µM for JURL-MK1). Results are expressed as percentages of the colonies counted in 0.1% DMSO-treated control groups. Data are the averages of three independent experiments made in duplicate (± standard error). **P ≤ 0,05, **P ≤ 0,01, ***P ≤ 0,001*

Considering the negative effect of autophagy induction for the therapeutic effects of imatinib and the potential inhibition of this process caused by celecoxib, we tested the effect of the two drugs, given in combination, on the clonogenicity of CML cell lines. As clearly shown in Figure 43 (upper panel), in LAMA-84 cell line, sub-optimal concentrations of celecoxib (250 nM) and imanitinib (10 nM), both close to the EC25 calculated through clonogenic assays, have an inhibitory effect on the formation of colonies, at least of additive nature. Although less evident, also in JURL-MK1 cells was observed a potentiation of the effect caused by imatinib when adding celecoxib at concentrations close to their EC25 calculated for this cell line (respectively 20 nM for imatnib, and 3 μM for celecoxib) (Figure 43, lower panel).

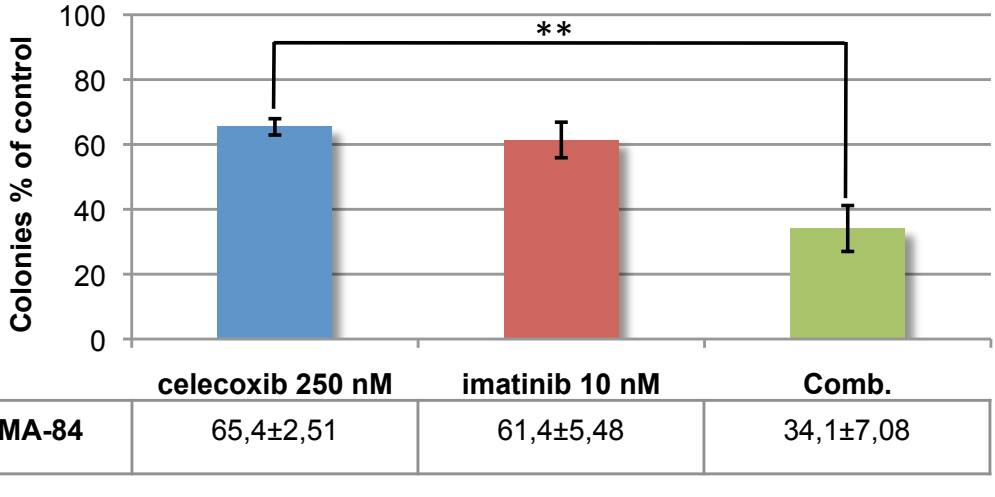

LAMA-84	65,4±2,51	61,4±5,48	34,1±7,08

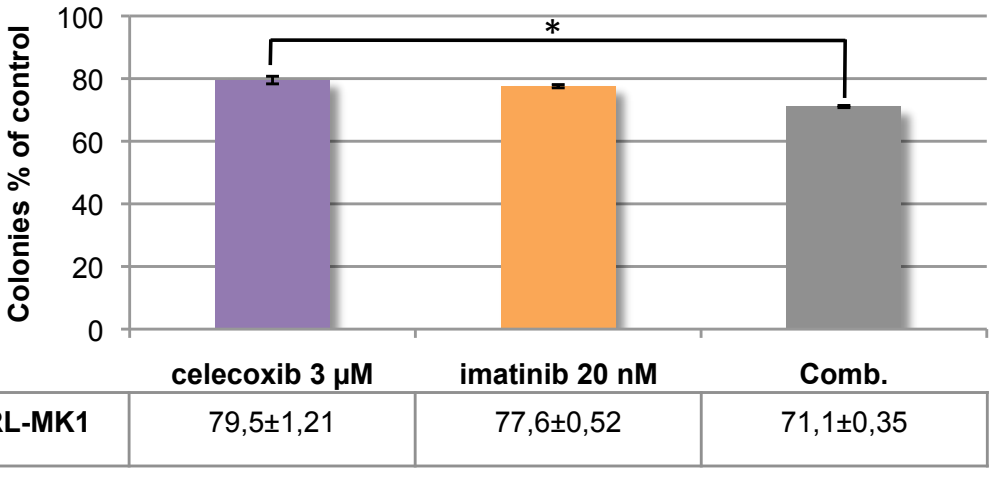

JURL-MK1	79,5±1,21	77,6±0,52	71,1±0,35

Figure 43. Celecoxib potentiates the anti-leukaemic effect of imatinib on CML cell lines.

Concentrations near the EC25 of celecoxib (see Figure 42) or of imatinib (10 nM for LAMA-84; 20 nM for JURL-MK1) were chosen for 6 days on the base of clonogenic assays previously performed. Drugs were administered alone or in combination (**Comb.**). Results are expressed as the percentages of the colonies counted in 0.1% DMSO-treated control groups. Values are the means of three independent experiments made in duplicate (± standard error). **P ≤ 0,05, **P ≤ 0,01, ***P ≤ 0,001* (*student t-test*).

Chapter 4:

Discussion

4. Discussion

Beyond their use as anti-inflammatory drugs, inhibitors of cyclooxigenase 2 (COXIB, and specifically celecoxib) were proposed as possible therapy for solid cancers, and specifically in the management of colon cancers [48,55]. This type of application found its rationale on the demonstrated ability of COXIB to selectively reduce the production of pro-flogistic arachidonic acid derivatives (prostaglandins, prostacyclins and leucotriens), which sustain inflammation as the pathogenic mechanism of cellular transformation in a large bowel affected by chronic colitis. Previous studies also demonstrated that over-expression of COX-2 in tumor cells enables various cancer-promoting effects, such as the over-expression of pro-angiogenic factors (VEGF, IL6, IL8), the activation of metalloproteases (MMP1, MMP2) and the resistance to apoptosis inducing stimuli, thus establishing a possible correlation between COX-2 activity and the impairment of apoptosis that characterizes many types of cancer [50,51].

Nevertheless, only celecoxib, amongst COXIBs, demonstrated this ability to impair cancer proliferation, including those tumor cells that do not express the COX-2 enzyme [53,54].

This opened the road to several studies attempting to identify alternative molecular mechanisms underlying the anti-cancer function of celecoxib.

Moving into this direction, we tested the ability of celecoxib to impair proliferation also of non-solid cancers, by studying the response of chromosome Philadelphia-positive (Ph+) Chronic Myelogenous Leukaemia cells bearing the 210 kDa isoform of the BCR-ABL oncogene, both in vitro and in vivo settings. Moreover, we also worked on defining the molecular mechanism of action of celecoxib.

In order to characterize this response, we evaluated the impact of celecoxib on cell viability and its mechanism of action by using three human cell lines, K562, LAMA-84 and JURL-MK1. MTT assays evidenced the ability of celecoxib to impair cell proliferation in a concentration-dependent manner, identifying in the LAMA-84 cell line the most sensitive to the anti-proliferative action of celecoxib (EC50 23,8 μM) (Figure 15a). Moreover, these data revealed that celecoxib induces a cytostatic rather than a cytotoxic effect, at least at concentrations below 25 μM, since MTT absorbance of celecoxib-treated cells were inferior to those recorded in control groups, without reaching levels smaller of the “zero” time-point (which corresponds to the number of cells at the moment of treatments with drugs; Figure 15a).

The anti-proliferative effects of celecoxib appeared also irreversible and time-dependent considering that the inhibition of cell growth caused by a single administration of the drug was more evident by increasing the length of exposure; indeed, the EC50 calculated six days after a single treatment, was consistently reduced (8,2 μM as calculated for LAMA84 and 23,8 μM for JURL-MK1) (Figure 15b).

In order to better understand the events underlying the anti-proliferative effect induced by celecoxib, we used the most responsive cell line, LAMA-84, to profile the cell cycle distribution. Thus, we established that after 24 hours in presence of celecoxib (25 μM)

most of the cells gathered in the G1 phase of the cell cycle, with a contemporary depletion in the S and, more evidently, in the G2 phases. Moreover, this treatment caused the emergence of apoptotic "bodies" identified as a SubG1 peak in the histogram that illustrates the distribution of single-cell DNA content. These data, which were also corroborated by the results of the trypan blue exclusion test and by microscopic counting of apoptotic nuclei, substantially confirmed previous reports on the effects of celecoxib on BCR-ABL-independent leukaemic cell lines (Jurkat, HL60, U937), which revealed a dose- and time-dependent inhibition of cell growth (with a G1-block of the cell cycle), and induction of apoptosis [48] (Figures 16, 17, 18).

Intriguingly, western blot analysis of COX-2 expression together with a comparison of COXIB (rofecoxib) and non-COXIB (di-methyl-celecoxib) analogues in assays evaluating their anti-proliferative potential, provided a strong evidence that celecoxib exerts its anti-leukaemic function in a COX-2-independent manner (Figures 20, 21). This is in agreement with the observations of other groups showing very similar growth inhibition patterns for celecoxib in COX-2 (+/+), (+/–) and (–/–) mouse embryo fibroblast and also in COX-2 negative hematopoietic cell lines, including K562 [49,52,68].

The most cited argument against the specificity of these anti-proliferative, COX-2-independent effects, of celecoxib is the need of very high concentrations, around 100 μM, of this drug. To this regard, we were able to obtain a substantial decrease in cell proliferation and viability already after 24h in presence of only 25 μM celecoxib while, an increase in the length of exposure to this drug, allows the use of even lower concentrations in order to achieve similar results. Furthermore, clonogenic assays were useful to demonstrate that celecoxib may be active even at concentration in the lower micromolar range, with an EC50 of 500 nM, as calculated using the LAMA-84 cell lines (Figure 22). These data are of great importance since it has been demonstrated that, in mice, plasmatic concentrations as high as 45 μM are well tolerated in vivo. Moreover, due to the lipophilic nature of celecoxib, this drug is concentrated three to four times more in bone marrow, where leukaemogenesis occurs, than in plasma; therefore, a concentration of 25 μM celecoxib in the hematopoietic compartment can be achieved using a dose of 950 mg, not to far from the daily dose commonly used in the treatment of Familial Adenomatous Polyposis (800 mg, divided in two administrations).

Another important aspect of innovation of the present work is the characterization of the molecular pathways involved in the effects of celecoxib onto CML blasts. Indeed, we demonstrated, by biochemical and genetic approaches, that β-catenin down-regulation is pivotal in the anti-leukaemic effect evoked by celecoxib, mainly relying on de-repression GSK-3β (Figures 23-30). Moreover, since BCR-ABL normally inhibits GSK-3β by an Akt-dependent phosphorylation of its ser-9 residue, our data demonstrate that celecoxib interferes directly with BCR-ABL oncogenic pathways. This may have important implications in the cure of CML patients since several groups have demonstrated that the Wnt/β-catenin/Tcf-Lef pathway is fundamental in maintaining the self-renewal capacity of LSCs. Indeed, its becoming clear that the Wnt/β-catenin/Tcf-Lef pathway is aberrantly activated in CML blasts during the chronic phase, when it specifically fuels the LSCs

towards excessive self-renewal, and, eventually, later on, toward the blast crisis evolution of the disease [14,17,18]. Moreover, Heidel et al hypothesized that inhibition of canonical Wnt signaling hampers the resistance to imatinib of CML stem cells, thereby maximizing the therapeutic outome of a conjunct treatment with imatinib. As regards these aspects, recent works demonstrated that, independently of Wnt function, BCR-ABL tyrosine kinase activity enables β-catenin-driven transcription, by both inhibiting its GSK-3β-dependent degradation and facilitating the interaction with Tcf/Lef transcription factors (directly phosphorylating of β-catenin) [19].

According to evidence in the literature [20], we found that celecoxib-induced restoration of GSK-3β, besides the impairment of the β-catenin/Tcf/Lef axis, causes the selective inhibition of mTORC1 assembling without a compensatory increase of mTORC2 (Figures 31, 32). Agreeing with this data, we observed a paradoxical but transitory increase in Akt phosphorylation on serine 473 following to treatments with celecoxib (data no shown), which can be explained with the removal of the feedback inhibition on the PI3K-Akt pathway normally exerted by mTORC1 [69]. Moreover, as regards the inhibition of cell proliferation, we demonstrated that the effects of celecoxib and PP242, an inhibitor of mTOR catalytic function, are not additive, suggesting a redundant mechanism of action (Figure 33).

Interestingly, previous studies provided evidence that S6K exerts a negative control on GSK-3β [32], thereby contributing to the oncogenic events that increase β-catenin levels. On the other hand, according to our data, celecoxib-induced abrogation of mTORC1 may be either the consequence of GSK-3β restoration or its cause. To this regard, the demonstration that celecoxib is able to rapidly (within minutes) activate AMPK (Figure 34) seems to suggest that the consequent inhibition of mTORC1 [66,70] remains upstream of GSK-3β restoration. At the same time, by knocking-down its expression, we demonstrated that AMPK is required for both β-catenin down-regulation and the antileukaemic effects of celecoxib (Figures 38, 39), suggesting that the activation of the serine/threonine kinase occurs very upstream in the cascade of events triggered by this drug.

Although, the demonstration that celecoxib causes AMPK phosphorylation in a CaMKKβ-dependent manner (Figures 35-37) implies that the immediate target of this COXIB has the capacity to influence intracellular Ca^{2+} concentrations. These data are in partial agreement with the work of Pyrko et al. [58,71], which demonstrates that celecoxib is able to induce the release of Ca^{2+} from endoplasmic reticulum (ER) stores, although, in our model, this event is not associated to the activation of ER stress response (data not shown).

Also in favour of a possible use in the therapy of CML, we demonstrated that celecoxib does not activate autophagy (Figure 40-42), conversely to what described for TKI [44,72]. More suggestively, serum and amino acid deprivation, which potently activates cell autophagy, was able to potentiate the antiproliferative response to celecoxib (data not shown), while co-administration of this COXIB with very low concentrations of imatinib (close to the EC25 calculated for each compound) display an inhibitory effect on cell proliferation that was at least of additive nature (Figure 43).

Of importance, thanks to a partnership with Dr. Bruno Calabretta's lab (Kimmel Cancer

Center, Thomas Jefferson University, Philadelphia, USA), we verified the antiproliferative function of celecoxib on CML blasts isolated from three different patients but not on $CD34^+$ hematopoietic progenitors, a result that strongly sustain the specificity of the action exerted by this COXIB on leukaemic cells (data not shown).
Finally, the conserved antiproliferative response to celecoxib, dimethyl-celecoxib, but not to indomethacine (an inhibitor of both COX-1 and COX-2), observed by Dr Calabretta's group in another BCR-ABL-dependent leukemia model, the acute lymphocytic leukaemia (ALL) cell line named BV173K, makes wider the horizon of the clinical applications of celecoxib; moreover, its ability to abrogate the clonogenicity of BV173K cells bearing the TKI-resistant T315I mutant of BCR-ABL suggests that celecoxib may be used to treat those patients left uncovered by the standard therapy.

Chapter 5:

References

References

- ([1]) Calabretta B. and Perrotti D. The biology of CML blast crisis. Blood, 2004; 103 (11): 4010-4021.
- ([2]) Melo Junia V., et al. Chronic Myeloid Leukemia. American Society of Hematology, 2003: 132-152
- ([3]) Mahon FX., et al. Selection and characterization of BCR-ABL positive cell lines with differential sensitivity to the tyrosine kinase inhibitor STI571: diverse mechanisms of resistance. Blood. 2000; 96: 1070-1079.
- ([4]) Hehlmann R., et al. Chronic myeloid leukaemia. Lancet 2007; 370: 342–50.
- ([5]) Druker Brian J. Translation of the Philadelphia chromosome into therapy of CML. Blood. 2008; 112(13): 4808-4817.
- ([6]) Hamad A., et al. Emerging Therapeutic Strategies for Targeting Chronic Myeloid Leukemia Stem Cells. Stem Cells International. Volume 2013:1-12.
- ([7]) Deininger Michael W. N., et al.The molecular biology of chronic myeloid leukemia. Blood, 2000; 112 (13): 3343-3356.
- ([8]) C.Fava, et al. Chronic Myeloid Leukemia: State of the Art in 2012. Curr Oncol Rep. 2012; 14:379–386.
- ([9]) Baghdadi Tareq Al., et al. Novel Combination Therapy Targeting Chronic Myeloid Leukemia Stem Cells. Clinical Lymphoma, Myeloma & Leukemia, 2012;12 (2): 94-105.
- ([10]) Keeshan K, et al. Elevated Bcr-Abl expression levels are sufficient for a haematopoietic cell line to acquire a drug-resistant phenotype. Leukemia, 2001;15:1823-1833.
- ([11]) Gorre ME, et al. Clinical resistance to STI-571 cancer therapy caused by BCR-ABL gene mutation or amplification.Science, 2001;293:876-880.
- ([12]) Crews Leslie A. et al. Selective elimination of leukemia stem cells: Hitting a moving target. Cancer Letters, 2013; 338:15–22.
- ([13]) Weissman I. Stem Cell Research. Paths to Cancer Therapies and Regenerative Medicine. American Medical Association, 2005; 294 (11):1359-1366.
- ([14]) Zhao C., et al. Loss of β-Catenin Impairs the Renewal of Normal and CML Stem Cells in Vivo. *Cancer Cell*. 2007; 12(6): 528–541.
- ([15]) Kühl Susanne J., Kühl Michael. On the role of Wnt/β-catenin signaling in stem cells. Biochimica et Biophysica Acta, 2013; 1830: 2297–2306.
- ([16]) Clevers Hans. Wnt/β-Catenin Signaling in Development and Disease. *Cell*, 2006; 127: 469-480.
- ([17]) Heidel Florian H., et al. Genetic and Pharmacologic Inhibition of β-Catenin Targets Imatinib-Resistant Leukemia Stem Cells in CML. *Cell Stem Cell*, 2012; 10: 412-424.
- ([18]) Kleppe M., Levine Ross L. Targeting β-Catenin in CML: Leukemia Stem Cell Beware. *Cell Stem Cell*, 2012; 10: 351-353.
- ([19]) Reddiconto G., et al. Targeting of GSK3 promotes imatinib-mediated apoptosis in quiescent $CD34^+$ chronic myeloid leukemia progenitors, preserving normal stem cells. *Blood*, 2012; 119 (10): 2335-2345.
- ([20]) Coluccia A., et al. Bcr-Abl stabilizes β-catenin in chronic myeloid leukemia through its tyrosine phosphorylation. The EMBO Journal, 2007; 26: 1456–1466.
- ([21]) Logan Catriona Y. Logan and Nusse R. THEWNT SIGNALING PATHWAY IN DEVELOPMENT AND DISEASE. Annu. Rev. Cell Dev. Biol, 2004; 20:781–810.
- ([22]) Xing Y, et al. Crystal structure of a beta-catenin/axin complex suggests a mechanism for the betacatenin destruction complex. *Genes Dev,* 2003*;* 17:2753–64.
- ([23]) MacDonald Bryan T., et al. Wnt/β-catenin signaling: components, mechanisms, and diseases. *Dev Cell*, 2009; 17(1): 9–26.
- ([24]) Fu Yuejun, et al. β-catenin as a potential key target for tumor suppression. Int. J. Cancer, 2011; 129: 1541–1551.
- ([25]) Clevers H. and Nusse R. Wnt/β-Catenin Signaling and Disease.

Cell, 2012; 127: 1192-1205.

- ([26]) Polakis P. The oncogenic activation of β-catenin. Current Opinion in Genetics & Development. 1999; 9:15-21.
- ([27]) Kollings Frank T., et al. Neoplastic Transformation of RK3E by Mutant β-Catenin Requires Deregulation of Tcf/Lef Transcription but Not Activation of c-*myc* Expression. MOLECULAR AND CELLULAR BIOLOGY,1999; 19(8): 5696-5706.
- ([28]) Li Vivian S.W. et al. Wnt Signaling through Inhibition of β-Catenin Degradation in an Intact Axin1 Complex. Cell, 2012; 149: 1245–1256.
- ([29]) Major MB, et al. Wilms tumor suppressor WTX negatively regulates WNT/beta-catenin signaling. Science 2007;316:1043–1046.
- ([30]) Sierra J, et al. The APC tumor suppressor counteracts beta-catenin activation and H3K4 methylation at Wnt target genes. Genes & development 2006; 20: 586–600.
- ([31]) Inoki K., et al. TSC2 Mediates Cellular Energy Response to Control Cell Growth and Survival. Cell, 2003; 115:577–590.
- ([32]) Zhang Hui H., et al. S6K1 Regulates GSK3 under Conditions of mTOR-Dependent Feedback Inhibition of Akt. Molecular Cell, 2006; 24:185–197.
- ([33]) Inoki K., et al. TSC2 Integrates Wnt and Energy Signals via a Coordinated Phosphorylation by AMPK and GSK3 to Regulate Cell Growth. Cell, 2006;126:955–968.
- ([34]) Choo Andrew Y., et al. Mind the GAP: Wnt Steps onto the mTORC1 Train. Cell, 2006; *126*: 834-836.
- ([35]) Julien Louis-Andre., et al. mTORC1-Activated S6K1 Phosphorylates Rictor on Threonine 1135 and Regulates mTORC2 Signaling. *Mol.Cell.Biol.* 2010;30(4):908-921.
- ([36]) Inoki K., et al. AMPK and mTOR in Cellular Energy Homeostasis and Drug Targets. Annu. Rev. Pharmacol. Toxicol. 2012;52:381-400.
- ([37]) Gwinn Dana M. et al. AMPK Phosphorylation of Raptor Mediates a Metabolic Checkpoint. Molecular Cell. 2008; 30: 214–226.
- ([38]) Woo Lee J., et al. The Association of AMPK with ULK1 Regulates Autophagy. PLoS ONE. 2010; 5(11):1-9.
- ([39]) Gormand A., et al. Regulation of AMP-Activated Protein Kinase by LKB1 and CaMKK in Adipocytes. Journal of Cellular Biochemistry. 2011;112:1364–1375.
- ([40]) Leclerc Gilles M., et al. AMPK-induced activation of Akt by AICAR is mediated by IGF-1R dependent and independent mechanisms in acute lymphoblastic leukemia. Journal of Molecular Signaling. 2010; 5:15.
- ([41]) Vakana E., et al. Antileukemic effects ofAMPK activators on BCR-ABL–expressing cells. Blood. 2011, 118 (24): 6399-6402.
- ([42]) Yu Li,et al. The selectivity of autophagy and its role in cell death and survival. Autophagy. 2008; 4(5): 567-573.
- ([43]) Xie Zhiping and Klionsky Daniel J. Autophagosome formation: core machinery and adaptations. Nature Cell Biology, 2007; 9:1102 –1109.
- ([44]) Bellodi C, et al. Targeting autophagy potentiates tyrosine kinase inhibitor–induced cell death in Philadelphia chromosome–positive cells, including primary CML stem cells. The Journal of Clinical Investigation. 2009; 119(5):1109-1123.
- ([45]) Chen N. Debnath J. Autophagy and tumorigenesis. FEBS Letters.2010;584(7):1427-35.
- ([46]) Puissant A., et al. Resveratrol Promotes Autophagic Cell Death in Chronic Myelogenous Leukemia Cells via JNK-Mediated p62/SQSTM1 Expression and AMPK Activation. *Cancer Res* 2010;70:1042-1052.
- ([47]) Robin Mathew, et al. Role of autophagy in cancer. Nature reviews. 2007, Nature Publishing Group; 7:961-967
- ([48]) Ping Pang R., et al. Celecoxib induces apoptosis in COX-2 deficient human gastric cancer cell through Akt/GSK-3β/NAG-1 pathway. Cancer Letters, 2007; 251: 268–277.
- ([49]) Subhashini J., et al. Anti-proliferative and apoptotic effects of celecoxib on human

chronic myeloid leukemia in vitro. Cancer Letters, 2005; 224: 31–43.

- ([50]) Arunasree Kalle M., et al. Imatinib resistant K562 cells are more sensitive to celecoxib, a selective COX-2 inhibitor: Role of COX-2 and MDR-1. Leukemia Research, 2008; 32: 855-864.
- ([51]) RodJ. Flower. THE DEVELOPMENT OF COX2 INHIBITORS. Nature Reviews Drug Discovery, 2003; 2:179-191.
- ([52]) Sen Zhang G., et al. Antitumor effects of celecoxib on K562 Leukemia cells are mediated by cell-cycle arrest, caspase-3 activation, and downregulation of Cox-2 expression and are synergistic with hydroxyurea or imatinib. American Journal of Hematology, 2006; 81: 242-255.
- ([53]) Hanif R., et al. Effects of nonsteroidal anti-inflammatory drugs on proliferation and on induction of apoptosis in colon cancer cells by a prostaglandin-independent pathway. Biochem Pharmacol. 1996; 52: 237-245.
- ([54]) Goluboff E.T., et al. Olsson (sulinac sulfone) suppress growth of human prostate cancer in anude mouse xenograft model by increasing apoptosis. Urology, 1999; 53: 440-445.
- ([55]) Schönthal AH. Direct non-cyclooxygenase-2 targets of celecoxib and their potential relevance for cancer therapy. British Journal of Cancer, 2007; 97: 1465-1468.
- ([56]) Kardosh A, et al. Aggravated Endoplasmic Reticulum Stress as a basis for enanched Glioblastoma cell killing Bortezomib in combination with celecoxib or its non-coxib analogue, 2,5-Dimethyl-Celecoxib Cancer Res, 2008; 68 (3): 843-851.
- ([57]) Kardosh A, et al. Dimethyl-Celecoxib (DMC), a Derivative of Celecoxib that Lacks Cyclooxygenase-2-Inhibitory Function, Potently Mimics the Anti-Tumor Effects of Celecoxib on Burkitt's Lymphoma In Vitro and In Vivo. Cancer Biology & Therapy, 2005; 4:5, 571-582.
- ([58]) Pyrko P. et al. Calcium-activated endoplasmic reticulum stress as a major component of tumor cell death induced by 2,5-dimethyl-celecoxib, a non-coxib analogue of celecoxib. Mol Cancer Ther, 2007; 6(4): 1262-1275.
- ([59]) Mainer T.J, et al. Targeting the beta-catenin/APC pathway: a novel mechanism to explain the cyclooxygenase-2-independent anticarcinogenic effects of celecoxib in human colon carcinoma cells FASEB Journal, 2005.
- ([60]) Song X., et al. Cyclooxygenase-2, player or spectator in cyclooxygenase-2 inhibitor-induced apoptosis in prostate cancer cells. J Natl Cancer Inst, 2002; 94: 585-591.
- ([61]) Schönthal AH. Antitumor properties of dimethyl-celecoxib, aderivative of celecoxib that does not inhibit cyclooxygenase-2: implications for glioblastoma therapy. Neurosurgical Focus, 2006; 20 (E21): 1–10.
- ([62]) Meade Barlow, et al. Celecoxib inhibits invasion and metastasis via a cyclooxygenase 2-independent mechanism in an in vitro model of Ewing sarcoma. Journal of Pediatric Surgery 2012;47:1223–1227.
- ([63]) Chen R, et al. Ubiquitin-mediated interaction of p210 BCR/ABL with β-catenin supports disease progression in a murine model for chronic myelogenous leukemia *Blood*; 2013 Aug 15 [Epub ahead of print].
- ([64]) B.W. Doble, et al. Functional Redundancy of GSK-3α and GSK-3β in Wnt/β-Catenin Signaling Shown by Using an Allelic Series of Embryonic Stem Cell Lines. Developmental Cell. 2007 June; 12,: 957–971.
- ([65]) Wassermann S,et al. p16INK4a is a beta-catenin target gene and indicates low survival in human colorectal tumors. Gastroenterology. 2009;136(1):196-205.
- ([66]) Joungmok K, Mondira K, Benoit V, Kun-Liang G. AMPK and mTOR regulate autophagy through direct phosphorylation of Ulk1. Nature Cell Biology. 2011;13(2):132-141.
- ([67]) Lum, J.J., et al. Growth factor regulation of autophagy and cell survival in the absence of apoptosis. *Cell.* 2005;120:237–248.
- ([68]) Williams CS., et al. Celecoxib prevents tumor growth in vivo without toxicity to normal gut: lack of correlation between in vitro and in vivo models. Cancer Res. 2000;60:6045-605.

- ([69]) Huang J and Manning Brendan D. A complex interplay between Akt, TSC2, and the two mTOR complexe. *Biochem Soc Trans*. 2009;37(Pt 1):217–222.
- ([70]) Chaudhary Sandeep C., et al. Metformin, an anti-diabetic agent reduces growth of cutaneous squamous cell carcinoma by targeting mTOR signaling pathway. Photochem Photobiol. 2012;88(5):1149–1156.
- ([71]) K. Tanaka, W. et al. Involvement of intracellular Ca2+ levels in nonsteroidal anti-inflammatory druginduced apoptosis, J. Biol. Chem. 2005;280:31059–31067.
- ([72]) Salomoni P. and Calabretta B. Targeted therapies and autophagy. Autophagy. 2009;5(7):1050-1051.

Acknowledgments (Ringraziamenti)

Grazie al Professor Fabrizio Condorelli per avermi concesso la possibilità di svolgere questo percorso di Dottorato nel suo laboratorio, permettendomi di coltivare la mia passione per la Ricerca e per tutti gli insegnamenti professionali e di vita che mi hanno permesso di crescere e che porterò sempre con me…

Grazie a Ilaria, la mia Collega, ma soprattutto Amica… per la splendida amicizia che si è creata fra noi… per tutto ciò che abbiamo condiviso e creato insieme in questi anni… per essermi stata accanto, per avermi incoraggiata e aiutata, per le nostre chiacchierate… per ogni singolo momento trascorso insieme… non avrei mai potuto desiderare una collega migliore e… sarà a dir poco strano lavorare senza di te… Mi mancherai Ila…

Grazie a tutti i colleghi che ho incontrato in questi anni: Virginia, Antonio, Dimitry, Roberta, Francesca, Sarah e Salvatore.

Grazie ai fanciulli… Simone e Laura… In bocca al lupo per la vostra laurea…

Un grazie particolare ad Ambra, Cristina e Marco… per tutti i momenti lavorativi e soprattutto "extra-lavorativi" che abbiamo condiviso…per le chiacchierate e le pause sigaretta… per avermi fatta sentire parte del vostro gruppo… Mi mancherete ragazzi…

Grazie a tutti i miei amici… in particolare…

A Giulia, la mia più cara amica, per esserci sempre in ogni situazione e circostanza, per essermi stata accanto in quest'anno molto difficile per me, per la sua allegria e per tutti i momenti spensierati che trascorriamo insieme…

A Chicco, il mio fratellino, perché nonostante passino gli anni, noi rimaniamo comunque gli stessi… e con te torno sempre un po' bambina…

Grazie alla mia famiglia…

Ai miei zii e ai miei cugini…

Ai miei nonni per i valori che mi hanno insegnato…

A mia zia, che mi protegge da lassù… per la sua incredibile forza… per la sua voglia di non mollare mai…

Grazie ai miei genitori, ai quali dedico questa tesi, per avermi permesso di raggiungere questo importante traguardo, per avermi sempre supportata e molto spesso anche sopportata, per i loro insegnamenti, consigli ed incoraggiamenti… e per la fiducia e la stima che mi hanno sempre dimostrato…

Beatrice